Comparative Analysis of Conventional and Compact Heat Exchangers for Next Generation Nuclear Reactors

A Thesis

Presented in Partial Fulfillment of the Requirements for the

Degree of Master of Science

with a

Major in Nuclear Engineering

in the

College of Graduate Studies

University of Idaho

by

Amey Shigrekar

Major Professor: Richard Christensen, Ph.D.

Committee Members: Michael McKellar, Ph.D.; Vivek Utgikar, Ph.D.;

David Arcilesi, Ph.D.

Department Administrator: Richard Christensen, Ph. D.

August 2018

Authorization to Submit Thesis

This thesis of Amey Shigrekar, submitted for the degree of Master of Science with a major in Nuclear Engineering and titled "Comparative Analysis of Conventional and Compact Heat Exchangers for Next Generation Nuclear Reactors," has been reviewed in final form. Permission, as indicated by the signatures and dates given below, is now granted to submit final copies to the College of Graduate Studies for approval.

Major Professor: _____Date_____
Richard Christensen, Ph.D.

Committee Members: _____Date_____
Michael McKellar, Ph.D.

_____Date_____
Vivek Utgikar, Ph.D.

_____Date_____
David Arcilesi, Ph.D.

Department Administrator: _____Date_____
Richard Christensen, Ph.D.

Abstract

Advanced reactor concepts such as the Generation IV rectors were designed with the intent to achieve longer operational life cycles, a sufficiently high degree of safety, and a competitive economic edge over their fossil fuel-based energy producing counterparts. The design features of these reactors include higher fuel burn-ups, broader range of acceptable fuels, and high reactor coolant outlet temperatures. In order to utilize the heat produced by these reactors more efficiently, it is envisioned to couple them with various industrial process heat applications. However, transferring heat from the cores of these high temperature reactors requires high integrity heat exchangers (HXs) which can perform under severe conditions with high effectivenesses. Compact HXs have gained recent attraction due to their superior performance at high temperatures and pressures, as well as their capability to meet the needs of the myriad of industrial applications. This thesis primarily focuses on the comparison of such highly efficient compact HXs with the current industry standard conventional HXs, by gauging their thermal performance and economic benefits, to provide a stronger case for their large scale development and deployment.

In this study, two compact HXs, namely the printed circuit heat exchangers (PCHEs) with straight and zigzag channels, have been compared to a conventional tube-in-tube helical coil heat exchanger (HCHE). Various fluid sets with specific operating conditions were chosen to perform a design analysis, in order to acquire metrics for characterizing the thermal performances of the HXs, which was then followed by a simplistic cost analysis. MATLAB was used, to optimize the HX designs by iteratively solving the geometry-specific thermal hydraulic correlations, until the boundary conditions were met. Using the operating conditions for each fluid set, the assumptions made to simplify the analyses, and the applied design constraints, optimum HX designs were acquired.

Acknowledgements

I must first thank sincerely my parents, my sister and Priyanka, for their unwavering support and affection throughout the years. This would not have been possible without you. Next, I wish to express my deepest gratitude to my advisor Dr. Richard Christensen for his expert guidance, valuable insight and constant help during the course of this study. His patience, motivation and immense knowledge, has helped me in all the time of research and writing of this thesis.

I am very thankful to my committee members, Dr. Michael McKellar, Dr. Vivek Utgikar, and Dr. David Arcilesi, for their passionate participation, invaluable comments,m and constructive criticism which have improved my technical skills and understanding of the subject matter, as well as helped shape this thesis.

I would also like to thank Dr. Piyush Sabharwall who has been working with me on this project since its inception. He was the source of the inspiration to conduct this study. And finally, I would like to thank my friends Jieun Lee and Michael Shaltry, for making these years as a graduate student worthwhile.

Table of Contents

List of Tables

List of Figures

Nomenclature

A	heat transfer area
A_{cs}	flow cross sectional area
$\bar{C}$	heat exchanger compactness
c_p	specific heat at constant pressure
d_c	channel diameter
D_c	coil diameter
D_h	hydraulic diameter
d_i	inner tube diameter
d_o	outer tube diameter
f	Fanning friction factor
h	convective heat transfer coefficient
k	thermal conductivity
L_{HX}	calculated length of heat exchanger
L_{ch}	calculate length of heat exchanger channels
$\dot{m}$	fluid mass flow rate
N_c	number of channels
Nu	Nusselt number

ΔP	pressure drop
p_l	pitch length
p_t	channel pitch
P_c	perimeter of a single channel
P_w	wetted perimeter
Pr	Prandtl number
$\dot{Q}$	thermal duty of heat exchanger
$\dot{Q}_{max}$	maximum possible heat transfer rate
Re	Reynolds number
T	temperature
$\Delta T_1, \Delta T_2$	terminal temperature differences
ΔT_{lm}	log-mean temperature difference
t_e	effective thickness
t_p	plate thickness
U	overall heat transfer coefficient
v	mean fluid velocity
$\dot{W}$	pumping power
w_c	coil width
w_e	effective width

Greek Symbols

ϵ	heat exchanger effectiveness
η	dynamic viscosity
ϕ	pitch angle
ρ	fluid density

Subscripts

c	cold
$crit$	critical
f	fluid
h	hot
i	inner
in	inlet
l	laminar
o	outer
out	outlet
t	turbulent
tr	transitional
w	wall

CHAPTER 1

Introduction

1.1 Background

The U.S. Energy Information Administration's latest International Energy Outlook 2017 Report projects that world energy consumption will grow by 28% between 2015 and 2040. Most of this growth is expected to come from countries that are not in the Organization for Economic Cooperation and Development, and especially in countries where demand is driven by strong economic growth, particularly in Asia. Renewable energy, although the fastest-growing source of clean energy along with nuclear power, their combined projected growth is a meager 3.7% per year till 2040 [1]. There is a clear need for expansion of clean energy sources in order to replace fossil fuel power plants that are currently expediting the detrimental effects of climate change by emitting large amounts of carbon dioxide (CO_2). Additional energy sources are also required to meet the electricity demands of developing nations. This challenge for energy expansion has been taken up by the renewable and nuclear energy providers all over the world.

As of today, nuclear energy provides about 11% of the world's electricity from about 450 operational power reactors [2]. This is mainly produced by the currently operating Generation II and Generation III reactor designs, and although these reactors remain the popular choice of technology, the focus of the nuclear industry has been shifted towards the research and development of Generation IV (Gen IV) reactors. This shift is mainly due to the additional benefits that the advanced Gen IV reactors provide. The Gen IV reactors are a set of six reactor design concepts that were developed by the Generation IV International Forum, with the intent to achieve longer operational life cycles, a sufficiently high degree of safety, and a competitive economic edge when compared to their fossil fuel-based energy producing counterparts [3]. These designs

have salient features such as higher fuel burn-ups, broader range of acceptable fuels, passive safety features and relatively high reactor-coolant exit temperatures. High coolant temperatures are attractive as they lead to the possibility of coupling the nuclear power plants (NPPs) with industrial process heat applications, such as steam methane reforming, high temperature steam electrolysis for hydrogen production, and ammonia production [4], [5]. This allows for better utilization of the reactor heat, therefore enhancing the overall nuclear power cycle efficiency. However, the rise in temperature also demands the requirement of components that can operate under severe conditions. One such critical component, which is responsible for transferring heat from the primary reactor coolant to the secondary coolant, as well as between streams within the power cycles, is the heat exchanger (HX) [6].

1.2 Literature Review

Current existing designs for HXs in NPPs, herein termed as conventional HXs, have been in existence for a very long time, and are broadly classified in two categories; shell-and-tube HXs and helical coil heat exchangers (HCHEs). However, over the last few decades there has been a substantial amount of research on HX designs that are smaller in size and have higher heat transfer surface area densities. These designs were a result of the needs for reduction in energy consumption, capital investment minimization, as well as the rise in versatility of applications that require HXs [7]. One of the categories of the compact HXs, called the printed circuit heat exchangers (PCHEs), has stood out due to its high effectiveness, high thermal performance and ability to perform under high pressures [8]. Some of the significant research that has been conducted on PCHE designs, around the world, is presented below.

Nikitin et al. investigated the heat transfer and pressure drop characteristics of a PCHE for an experimental supercritical CO_2 (SCO_2) loop [9]. The HX test section

designed for a 3 kW heat load had its inlet fluid temperature varied from 280 to 300 °C, and pressure from 2.2 to 3.2 MPa for the hot side, and the inlet temperature from 90 to 108 °C, and pressure from 6.5 to 10.5 MPa for the cold side. Based on the results acquired, empirical correlations were derived to predict the heat transfer coefficients and pressure drops as functions of Reynolds number. The HX performance provided an overall heat transfer coefficient ranging between 300 - 650 W/m^2-K, and a heat transfer surface area density, also known as HX compactness, of approximately 1050 m^2/m^3. In conclusion, the authors suggested that the PCHE design was a promising compact HX for various applications with SCO_2 as the working fluid. Another study conducted by the same researchers also compared a hot water supplier used for industrial and commercial purposes, to a PCHE design having an S-shaped fin configuration, with SCO_2 as the primary fluid [10]. The hot water supplier considered for this study was the Japanese EcoCute residential water heater, which compresses CO_2 to about 10 MPa via adiabatic compression, and then transfers heat to water through a shell and tube HX. This study determined the fin and plate configurations for the PCHEs based on 3D modeling and CFD simulations, and concluded that the PCHE design required about 3.3 times lesser volume and produced a lower pressure drop by about 37% on the hot side, and about 10 times lesser on the cold side, when compared to the industrial hot water supplier.

In order to investigate the performance of compact HXs under conditions similar to those for a very high temperature reactor, Mylavarapu et al. designed, constructed and tested two PCHE designs that operated at fluid temperatures of up to 900 °C and pressures of about 3 MPa [11]. Using the high temperature test facility developed at The Ohio State University, a detailed investigation on various high temperature materials was carried out to aid the design of the HXs. Based on the results from the experimental and computational studies performed, correlations for determining the entrance length for a semicircular channel geometry, and the friction factor for entrance region laminar

flow were developed. The results also concluded that the material most suitable for PCHE designs, with Helium as their working fluid, was Alloy 617. Based on the design, construction and testing of the PCHEs, it was concluded that diffusion bonded HXs are promising candidates for high temperature heat transfer applications.

Kim et al. conducted numerical analysis of PCHEs to be used as intermediate HXs in high temperature gas reactors (HTGRs), mainly focusing on the wavy or zigzag channeled designs [12]. The researchers developed correlations for the Fanning friction factor and the Nusselt number, which included coefficients that were pitch angle dependent. The study varied the pitch angles from 5° to 45°, with 5° increments. A simplified cost analysis was also performed taking into account the capital cost, based on the material requirement, and the operating cost, based on the pumping power, in order to optimize the HX designs.

In contrast to high temperature experiments, PCHEs have also been studied for low temperature heat exchange scenarios. A study conducted by Baek et al. investigates the thermal hydraulic performance of PCHEs for cryogenic temperatures [13]. The researchers fabricated compact PCHEs with multiple corrugated micro-channels and used Helium as the working fluid, operating between temperatures of -196 to 27 °C. The study compared two designs; one with 250 layers of etched plates and other with 500 layers, and investigated the effects of the amount of material on axial thermal conduction.

1.3 Motivation

From the literature review presented in Section 1.2, it can be seen that the range of studies performed for PCHE designs is very extensive and diverse. However, there currently aren't any studies that compare the conventional and compact HXs to each other. This is the motivation behind performing the comparative analysis presented herein.

As of today, conventional HXs such as HCHEs and shell and tube HXs, are used for steam generation as well as intermediate heat exchange scenarios. These HX designs are relatively large in volumes leading to low compactness, they have moderate effectivenesses, and are highly susceptible to fouling, leading to higher maintenance costs. Traditional power plants only require a few units of these large HXs in order to meet all their heat transfer requirements. As a result, any downtime due to maintenance of the heat transfer system might lead to the possibility of the power generation cycle to be taken off-line, leading to financial losses to the power plant. For example, a single day of downtime for a NPP, producing about 1000 mega-watts of electricity, can cost roughly over 2 million USD [14].

In contrast, compact HXs have high effectivenesses, low heat losses and high heat transfer surface densities. Most of these HXs have fluid strainers to block debris from entering the channels, and are designed with the intent to allow fast cleaning to treat fouling issues [8]. Due to their relatively small sizes, a large number of these HXs can be connected in parallel to perform heat transfer functions. This has the additional benefit of allowing some of the HX modules to act as backups in the event that other HX units were to be taken off-line for maintenance. The other salient feature of compact HXs is that they generally operate within the laminar flow regime, thus leading to low pressure drops and therefore lower operational costs. It is clear that in order to enhance the overall performance of a NPP in terms of operations and economics, it is vital to replace the conventional HXs with advanced compact HX designs. However, a large scale deployment of compact HXs requires considerable modeling and testing of the designs, with a significant number of possible scenarios that the HXs are expected to perform under. These studies would provide concrete evidence in support of the superiority of compact HXs, and would help bridge the knowledge gap in HX technology required to construct highly efficient power cycles.

1.4 Goal

The primary focus of this study was to conduct a preliminary analysis on steady state designs of compact HXs, and compare their thermal performance, compactness, and other developed figures of merit (FOMs), with conventional HXs. This would quantify their higher performance, highlight their superiority, and support their large scale development and deployment. The ultimate goal of this study was to provide a simplistic model that is capable of performing quantifiable analysis, and providing metrics that the HX performances could be gauged on.

1.5 Approach

A comparison was drawn between compact and conventional HX designs, namely PCHEs and a tube-in-tube HCHE. The reason straight and zigzag channeled PCHEs were chosen was because they are the most established designs. In the case of the conventional HX, a tube-in-tube HCHE was picked because that was the design used in Fort St. Vrain nuclear reactor, which was one of the two HTGRs ever to be operated in the United States [15]. This is of particular interest because some of the advanced HTGRs have derived their designs based of the Fort St. Vrain nuclear reactor, and also plan on using HCHEs as their intermediate HXs [16]. For the analysis, a thermal duty of 400 MW was selected as it is comparable to the thermal rating of the Integral Molten Salt Reactor [17], which is a small modular Gen IV reactor design. The study included various fluid sets in order to use the acquired results, and further the analysis with the inclusion of different power cycles for future work. The power cycles of interest were the Helium Brayton Cycle and SCO_2 Brayton Cycle, because they are high efficiency power cycle candidates, to be coupled with two of the of advanced nuclear reactor designs; namely HTGRs and molten salt reactors (MSRs).

A steam Rankine cycle, which would have analyzed a Water-Water heat exchange was not considered for this study mainly for the reason that compact HXs would not perform optimally as steam generators. This is because of the significant increase in fluid volume due to phase change of water into steam. Taking into account the geometry of the PCHE channels, which are usually small in diameter, a large change in volume might result in choked flow in the HX, thus reducing its thermal performance. Another reason was based off the study conducted by Shin et al. wherein the author suggested that at high temperatures and pressures, density-wave oscillations would lead to instabilities in the steam flow and lead to large pressure drops in the HX [18]. Therefore, the analysis of a steam Rankine cycle was not looked at for this study. The fluid sets considered for analysis are provided in Table 1.1

Table 1.1: Fluid sets for heat exchanger design analysis

Fluid Sets	Power Cycle	Reactor Type
He-He	Helium Brayton Cycle	HTGR
He-SCO_2	Supercritical CO_2 Brayton Cycle	HTGR
FLiNaK-He	Helium Brayton Cycle	MSR
FLiNaK-SCO_2	Supercritical CO_2 Brayton Cycle	MSR
$KFZrF_4$-He	Helium Brayton Cycle	MSR
$KFZrF_4$-SCO_2	Supercritical CO_2 Brayton Cycle	MSR

Due to the reasons mentioned above, the intent was to model the HXs mainly as intermediate HXs and not steam generators. Helium and SCO_2 were considered for this study as they have great potential as working fluids for HTGRs. The two salts FLiNaK and $KFZrF_4$ were chosen for this study as they are of particular interest as potential candidates for MSRs.

1.6 Thesis Outline

Chapter 1 presents some background on the current status of HX technology, literature related to the research that has been conducted on compact HXs, the motivation behind

conducting this comparative analysis, as well as the goal of this study and the approach taken to achieve it. Chapter 2 provides an overview of the theory of the HXs chosen for this analysis, by describing their geometry and providing the methodology followed to perform sizing calculations. Chapter 3 details the mathematical models that were developed to acquire the thermal performance and sizing parameters, and Chapter 4 discusses the results of the same. Chapter 5 uses the results to perform a simplistic cost analysis and lastly, Chapter 6 concludes this study and summarizes the results acquired, with recommendations for future work.

CHAPTER 2

Heat Exchanger Theory

2.1 Overview

This chapter provides an overview of HX technology along with detailed description of the geometries of the HX designs considered for this study. The methodology described herein lists the assumptions that were made to simplify the analyses, the operating conditions of the fluid sets used, and boundary conditions used to constrain the HX sizing problem. This chapter also provides an overview of the procedure followed to perform the thermal hydraulic analyses for the HX designs.

Compact HXs can be characterized by their high heat transfer surface area densities and relatively small sizes, when compared to other HX types. The compactness for PCHEs usually ranges from 300 m^2/m^3 when operating liquid or two phase fluid streams to about 700 m^2/m^3 for gas streams [19]. Although compact HXs are not a new technology, with gasketed plate HXs being some of the earlier designs, their use was fairly limited and they were only reliable, as long as the integrity of the gaskets held up [20]. However, in recent years, technologies such as diffusion bonding have given rise to highly robust and compact HXs such as PCHEs. Due to their unique design and manufacturing process, diffusion bonded PCHEs are capable of performing at extremely high temperatures and pressures. Figure 2.1 shows a comparison between the operating ranges of diffusion bonded PCHEs and standard conventional HXs.

A process called photochemical etching has allowed for the freedom to choose a channel geometry that would result in high heat transfer rates [21]. Some of the prominent channel geometries include straight channel, wavy or zigzag channels, offset-strip finned channels and airfoil finned channels. These etched plates are stacked on top of each other and diffusion bonded at temperatures usually within 50% - 80% of the material's absolute

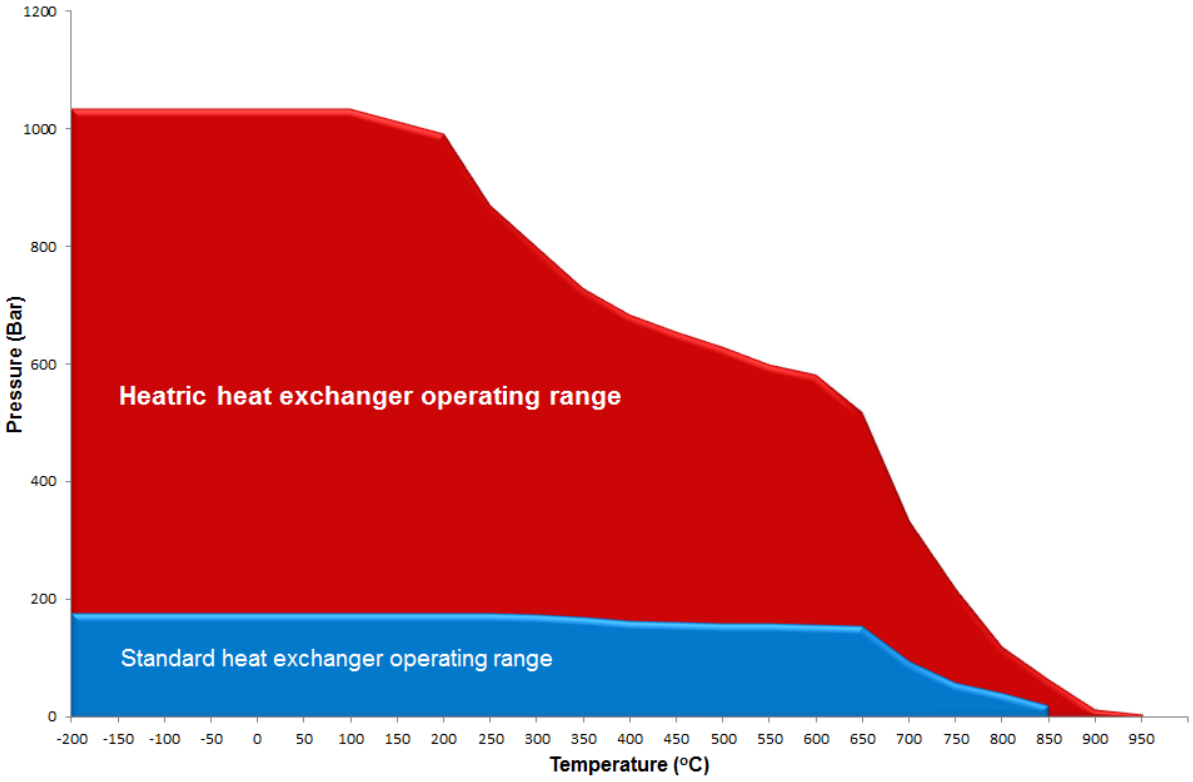

Figure 2.1: Operating range of PCHE designs

melting point. The end result is a solid block HX core with no joints or welds, which has exceptional strength and integrity, as well as high efficiency and enhanced thermal performance [8]. This study focuses on two compact HXs, namely the straight and the zigzag channeled PCHEs.

A 3-dimensional schematic of a PCHE can be seen in Figure 2.2. The counter-flow pattern indicated by the red and blue arrows is displayed along the cuboid that represents the HX core, manufactured by stacking and diffusion bonding a number of etched plates. The hot and cold fluids flow through channels in alternating plates, resulting in a design where a hot fluid flow plate is stacked between two cold fluid flow plates, and vice versa. The schematic also displays a view of a single heat transfer unit cell from the HX block, comprising of one hot and one cold channel, along with a cross sectional view of the same. The dimensions for the PCHE channels used in this study are provided in Table 2.1.

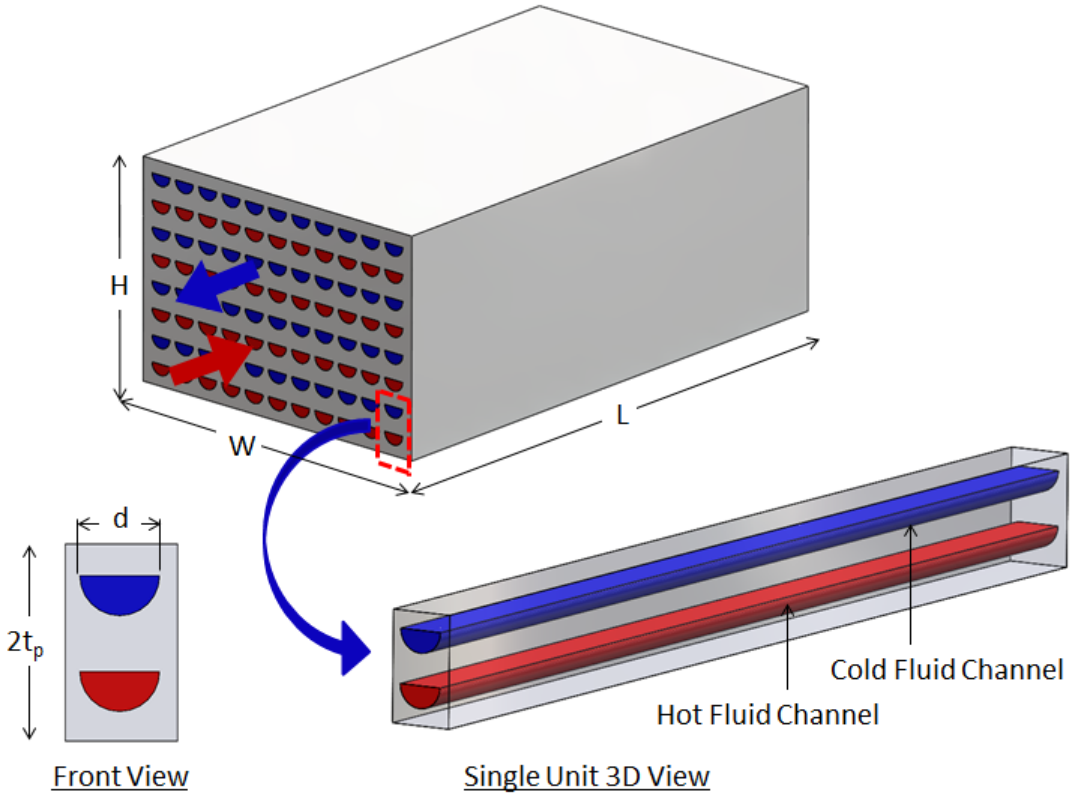

Figure 2.2: Schematic of a counter-flow straight channeled PCHE

Another variation of the compact HX studied here is the zigzag channeled PCHE. Figure 2.3 displays the channel geometry in a single plate of the zigzag PCHE, and it also provides a 3D view of a single heat transfer unit cell, similar to that in Figure 2.2. Externally, both the PCHE blocks look the same as the plates are diffusion bonded into a solid HX core. For this study, the flow pitch angles in the zigzag PCHE were varied from 5° to 30°, with an increment of 5°. This was done to analyze the effect of pitch angle increment on the thermal performance and compactness of the HX, as well as to see whether there exists a pitch angle for which the HX design is optimum.

The conventional HX chosen in this comparative study is a tube-in-tube HCHE. Figure 2.4 provides a schematic of a single tube-in-tube HCHE. Commercially used HCHEs have a large bundle of such tubes, coiled helically with an external shroud to provide insulation.

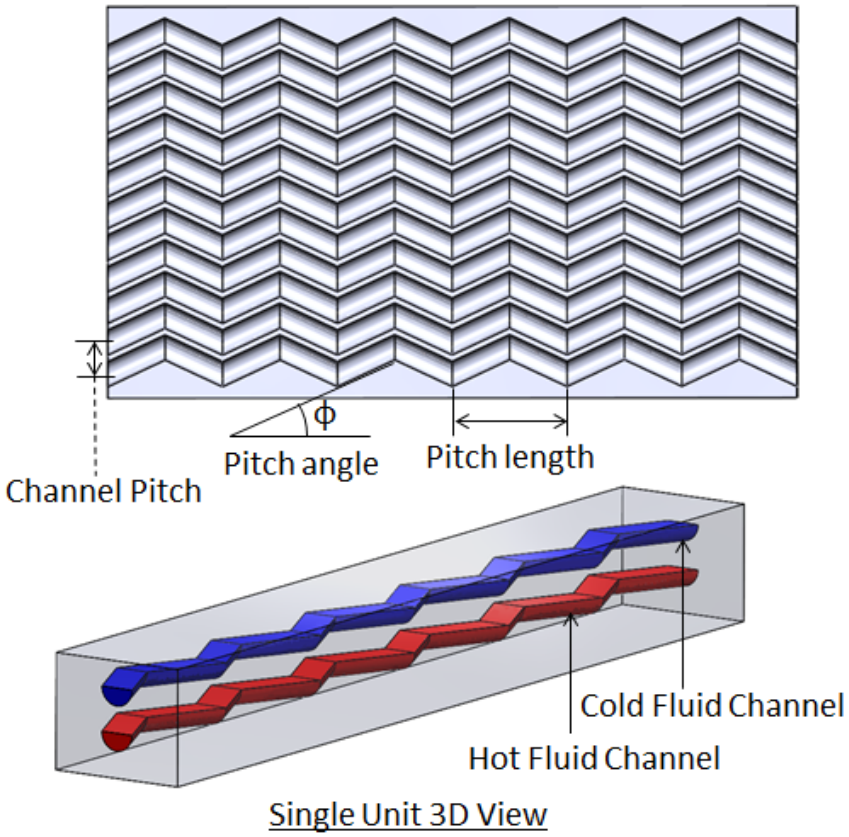

Figure 2.3: Schematic of a zigzag channeled PCHE

Table 2.1: Geometrical parameters of PCHE channels

Variable	Dimension
Channel diameter (d_c) [m]	0.002
Channel pitch (p_t) [m]	0.0025
Pitch angle, (ϕ)	Straight (0°), 5°, 10°, 15°, 20°, 25°, 30°
Pitch length, (p_l) [m]	0.0246
Plate thickness (t_p) [m]	0.00163
Hydraulic diameter (D_h) [m]	0.00122
Effective thicknes (t_e) [m]	0.000845
Effective width (w_e) [m]	0.002

A coiled bundle from a commercial HCHE is shown in Figure 2.5. Although the lengths of all the tubes will not be the same in such a bundled design, with the outermost tubes of the bundle being longer and the ones on the inner side being shorter, a thermal hydraulic analysis can be performed by assuming that the effect of the differences in the lengths

of tubes, on the HX performance can be averaged. Thus, a single tube analysis was considered during this study. The single tube dimensions were acquired from Sentry Equipment data sheet [22], and can be found in Table 2.2.

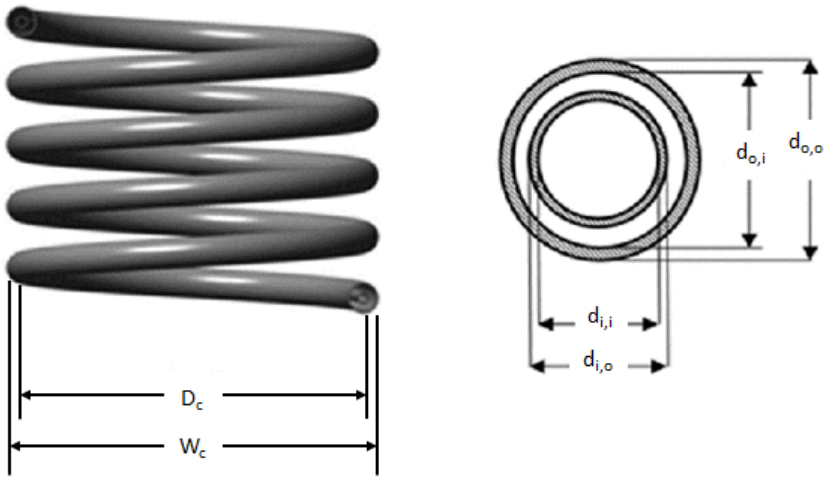

Figure 2.4: Schematic of a single tube-in-tube HCHE

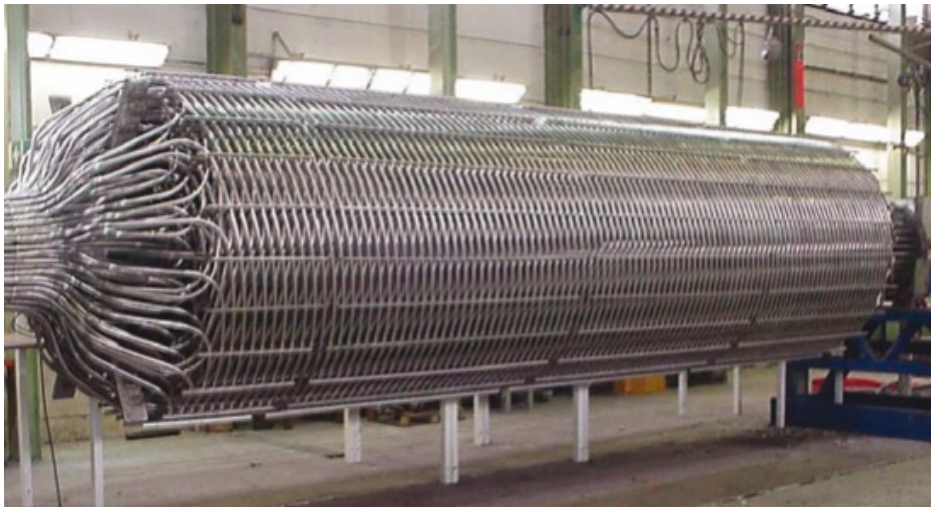

Figure 2.5: A bundle of helically coiled tubes in a HCHE [23]

Table 2.2: Geometrical parameters of HCHE tubes

Variable	Dimension
Inner tube ID ($d_{i,i}$) [m]	0.0102
Inner tube OD ($d_{i,o}$) [m]	0.0127
Outer tube ID ($d_{o,i}$) [m]	0.0212
Outer tube OD ($d_{o,o}$) [m]	0.0254
Coil Width (w_c) [m]	2.5
Diameter of curvature (coil diameter) (D_c) [m]	2.474

2.2 Methodology

The thermal hydraulic design and sizing process of HXs involves geometry dependent quantitative evaluations of the heat transfer and pressure drop characteristics. In this process, the HX type, constructional material, flow arrangement, and physical size is determined [24]. A sizing problem for HXs can be transformed into a rating problem by iteratively specifying the dimensions until the heat transfer performance and pressure drop requirements are met. This was the primary methodology followed while conducting the HX analyses for this study. The assumptions made to model the HXs and perform the sizing study were as follows

- No heat loss from the HXs to the surrounding.
- Heat transfer between adjacent heat transfer unit cells/tubes is ignored.
- Flow cross section for PCHEs is semicircular.
- Flow in PCHEs is fully developed laminar.
- HXs operate at steady state.
- Heat transfer is uniform throughout the HXs.

These assumptions helped simplify the design process and allowed for the sizing and thermal performance calculations. The wall material used for the construction of all the HXs in study was assumed to be Alloy 617. This material was chosen based on the studies conducted by Mylavarapu et al., wherein a detailed investigation was performed

on various alloys, to aid the design of PCHEs for high temperature operations. The density and the average thermal conductivity of this material were chosen to be 8360 kg/m^3 and 23 W/m-K, respectively [25]. The assumed effectiveness of the HXs was set to be 92%, as this is on the lower end of the PCHE performance and higher end of the HCHE performance parameter. For the fluid sets mentioned in Table 1.1, the operating conditions are provided in Table 2.3. These operating conditions were chosen by taking into consideration the general operating ranges within which the fluid sets perform for their respective reactor types. The thermophysical properties for the fluids were acquired from the National Institute of Standards and Technology's software called REFPROP, and a Nuclear Technology report on molten salt mixture properties [26].

Table 2.3: Operating temperatures and pressures of fluid sets

Fluid Sets	Temperatures (°C)			Pressures (MPa)	
	$T_{h,in}$	$T_{c,in}$	$T_{c,out}$	$P_{h,in}$	$P_{c,in}$
He-He	800	520	776	7	7
He-SCO_2	800	520	776	7	20
FLiNaK-He	750	530	725	0.1	7
FLiNaK-SCO_2	750	530	725	0.1	20
$KFZrF_4$-He	750	530	725	0.1	7
$KFZrF_4$-SCO_2	750	530	725	0.1	20

The three main constraints that were used as boundary conditions in the mathematical model were as follows

- Fully developed laminar flow (Reynolds Number $\leq$ 2200) in th case of PCHEs.
- PCHE maximum plate dimensions were to be 0.6 m in width, and 1.5 m in length.
- Maximum allowable pressure drops in the HXs should not exceed 1% of the operating pressures.

The fully developed laminar flow constraint was applied for PCHE sizing as the equations used to calculate the dimensionless numbers, such as Nusselt number and the Fanning friction factor are valid for that flow regime. The maximum allowable pressure drop

constraint is a standard specification in most HX designs, as it provides a ballpark value for the pressure drop that the pumping system is expected to overcome across the HXs. The maximum plate dimensions are set due to the fabrication capabilities of the company Heatric, that currently manufactures diffusion bonded PCHEs. The plate width is constrained by the dimensions of the photosensitive film necessary for the etching process, which is currently 0.6 m wide [27], and the maximum length of a manufactured HX plate as of date is 1.5 m. These constraints were used in the MATLAB code which solved the sizing problem iteratively.

Once the thermal hydraulic calculations of the HXs were concluded, the thermal performance parameters of the HX designs were used to develop the following FOMs

- FOM_1: Ratio of overall heat transfer coefficient to overall pressure drop.
- FOM_2: Ratio of overall pressure drop to length of HX channel.

These FOMs provided metrics in order to compare the thermal hydraulic performance of the HXs, taking into account the various HX geometries and the various fluid sets chosen for this study.

2.3 Calculation Procedure for Heat Exchanger Analysis

Taking into account the assumptions and the design constraints, the calculations carried out can be stated as follows

- Using the thermal duty requirement of 400 MW for the HX, the assumed effectiveness of 92%, and the operating conditions of the fluid streams as inputs, heat balance was conducted to calculate the fluid mass flow rates.
- From the acquired temperatures, the relationship between the heat transfer rate and the log-mean temperature difference (LMTD) was used to calculate the product

of the overall heat transfer coefficient and heat transfer area, UA. This product is also referred to as the thermal conductance.

- Using the dimensions of the channels in the PCHEs and dimensions of the tubes in HCHEs, the cross sectional flow areas were calculated.
- For PCHEs, the mass flow rates were used to calculate the number of channels required to maintain a laminar flow. This step was carried out to meet the first design constraint.
- Based on the number of channels required for laminar flow in PCHEs, the total cross sectional flow areas, as well as the per length total conduction areas of the HXs were calculated. The per length conduction areas when multiplied by the acquired lengths of the HXs would result in their total conductive heat transfer areas. In the case of HCHEs, the initial guess for number of tubes was set to 5000.
- Using appropriate correlations, dimensionless quantities such as Nusselt number and Fanning friction factors were calculated.
- The convective heat transfer coefficients were then calculated, based off which the overall heat transfer coefficient, U, was acquired. This calculation took into account the two convective heat transfer coefficients for the hot and the cold side, as well as the contribution to heat transfer via conductance.
- Knowing the overall heat transfer coefficient and the product UA, the heat transfer area, A, required to meet the thermal duty of the HXs was acquired.
- The lengths of HX channels were then calculated from the heat transfer areas, and the overall pressure drops were calculated based off the lengths.
- If the pressure drops exceeded 1% of the operating pressures, the number of channels acquired from preliminary calculations for the PCHEs, or the number of tubes assumed in the case of HCHEs as initial guesses was increased, and the above steps were repeated.

- These calculations were performed iteratively until the smallest HX designs satisfying all the constraints were acquired.

CHAPTER 3

Mathematical Modeling

This chapter discusses in detail, with relevant equations and correlations, the sizing and thermal hydraulic calculations mentioned in section 2.3. Most of the logic used to calculate the dimensions and FOMs for all three HXs in concern was similar, and therefore the generic equations are mentioned here before providing geometry specific correlations, which are explicitly described in the subsections of this chapter. The MATLAB code used to perform the calculations for all the three HX designs can be found in the Appendix.

The fixed parameters used as inputs include the duty of the HX, its effectiveness, the primary fluid inlet temperature, and the secondary fluid inlet and outlet temperatures. The primary fluid outlet temperature was calculated using the following methodology.

An initial guess for the outlet temperature of the primary fluid was made. It was assumed to be 5 °C hotter than the secondary fluid's inlet temperature in order to avoid a temperature cross in the HX. For steady state HX operation, the heat transfer rates, $\dot{Q}$, on the hot and the cold sides are given as follows

$$\dot{Q}_h = \dot{m}_h c_{p,h}(T_{h,in} - T_{h,out}) \tag{3.1}$$

and

$$\dot{Q}_c = \dot{m}_c c_{p,c}(T_{c,out} - T_{c,in}) \tag{3.2}$$

Here, $\dot{m}_h$ and $\dot{m}_c$ are the hot and cold fluid mass flow rates, and c_p represents the specific heat capacity of the fluids at constant pressures. As the heat transfer fluids were single phase in all cases, the thermophysical properties of the fluids were averaged over temperatures at the inlet and the outlet of the HXs. For an ideal situation with no heat losses to the surrounding, the heat lost by the hot fluid is equal to the heat gained by the cold fluid. Therefore

$$\dot{Q}_h = \dot{Q}_c = \dot{Q} \tag{3.3}$$

The heat capacity rate which is a product of $\dot{m}c_p$, is usually denoted by C. This simplifies Equations 3.1 and 3.2 to the following

$$\dot{Q}_h = C_h(T_{h,in} - T_{h,out}) \tag{3.4}$$

and

$$\dot{Q}_c = C_c(T_{c,out} - T_{c,in}) \tag{3.5}$$

The smaller of the hot and cold heat capacity rates was then used to acquire the maximum possible heat transfer rate, given as follows

$$\dot{Q}_{max} = C_{min}(T_{h,in} - T_{c,in}) \tag{3.6}$$

It can be seen that $\dot{Q}_{max}$ is a product of the minimum heat capacity rate, C_{min}, and the largest possible temperature difference in the HX. Equation 3.6 represents the heat transfer capability of a HX with an infinite surface area. It should be noted that C_{min} was used as it corresponds to the fluid with the lower heat capacity rate that would, in a hypothetically large HX, undergo the maximum possible temperature change. The HX effectiveness, which is the ratio of the actual heat transfer rate and the maximum possible heat transfer rate was then calculated as follows

$$\epsilon = \frac{\dot{Q}}{\dot{Q}_{max}} \tag{3.7}$$

If the calculated HX effectiveness was larger than the specified value of 92%, the initial guess value of the primary fluid outlet temperature was increased by 0.1 °C. This was performed iteratively until the HX effectiveness specification was met.

In a steady state heat transfer system, the maximum driving force for heat transfer between the primary and secondary fluids is the LMTD. This is generally given by

$$\Delta T_{lm} = \frac{\Delta T_1 - \Delta T_2}{ln\left(\frac{\Delta T_1}{\Delta T_2}\right)} \tag{3.8}$$

where ΔT_1 and ΔT_2 are temperature differences at the two ends of the HX, irrespective of the HX geometry, and ΔT_{lm} is the LMTD. For the counterflow scenario assumed for this study,

$$\Delta T_1 = T_{h,i} - T_{c,o} \tag{3.9}$$

and

$$\Delta T_2 = T_{h,o} - T_{c,i} \tag{3.10}$$

The heat transfer rate can also be written in terms of the thermal conductance, UA, and LMTD as follows

$$\dot{Q} = UA\Delta T_{lm} \tag{3.11}$$

The thermal conductance is useful as it can be related to the convective heat transfer coefficients of the working fluids and the conduction through the HX body. This concludes the generic calculations conducted to acquire the parameters to be used in the iterative part of the code. The following sections describe the HX geometry specific calculations that were performed for the compact and conventional HXs.

3.1 Calculations for PCHE

Hydraulic diameter is useful when dealing with fluid flows in pipes, ducts or conduits of various shapes. It helps simplify the use of a single variable rather than a set of variables,

while calculating dimensionless quantities such as Reynolds number, Nusselt number and friction factors. By definition, the hydraulic diameter is

$$D_h = \frac{4A_{cs}}{P_w} \tag{3.12}$$

where A_{cs} is the cross sectional area of the flow channel, and P_w is its wetted perimeter. For PCHEs, the channel geometry was assumed to be semicircular, as also shown in Figures 2.2 and 2.3, for which the hydraulic diameter using Equation 3.12 becomes

$$D_h = \frac{\pi d_c}{\pi + 2} \tag{3.13}$$

where d_c is the channel diameter. This definition was used while calculating dimensionless numbers, convective heat transfer coefficients and pressure drops for the PCHE systems.

Referring back to the design constraints, the first condition to be satisfied, for the PCHE sizing problem was for the flow to be fully developed laminar. In order to make sure that the HX geometry would satisfy this constraint, the mass flow rates of the hot and cold fluid streams were used to calculate the number of channels that would be required for the Reynolds number to be less than or equal to 2200. This was done for the hot and cold side individually, as the calculated mass flow rates and viscosities of both the fluids streams were different, and they would therefore result in a different number of channels. Once the number of channels for the hot and cold sides was calculated, the maximum of the two values was used in the hydrodynamic calculations that followed. This assured that the flow conditions for both the streams were fully developed laminar. Following this, the thermal hydraulic calculations were performed by using appropriate channel geometry-specific correlations.

The Nusselt number, *Nu*, for a fully developed laminar flow in straight channeled HXs, as suggested by Hesselgreaves [28], is given as follows

$$Nu = 4.089 \tag{3.14}$$

For zigzag channels, a modified correlation as proposed by Kim and No [12] was used, which is given as follows

$$Nu = 4.089 + cRe^{d} \tag{3.15}$$

Here, Re is the Reynolds number, and c and d are coefficients that depend on the channel diameter, the pitch angle, and the pitch length of the zigzag channels. The coefficient values are provided in Table 3.1 along with their respective root mean square errors (RMSEs). For fully developed laminar flow in straight channels, the Fanning friction factor, f, as suggested by Hesselgreaves [28] is given as follows

$$fRe = 15.78 \tag{3.16}$$

and for zigzag channels, the modified correlation proposed by Kim and No [12] is given as follows

$$fRe = 15.78 + aRe^{b} \tag{3.17}$$

The values for coefficients a and b are tabulated in table 3.1 along with their RMSEs.

Table 3.1: Kim's fitting constants for zigzag channeled PCHEs

Pitch Angle (ϕ)	a	b	RMSE (%) Fanning	c	d	RMSE (%) Nusselt
5°	0.0034	1.0502	2.343	0.00071	1.10341	3.024
10°	0.02342	0.8863	1.942	0.00314	0.96567	0.482
15°	0.06677	0.81258	1.591	0.0083	0.86054	0.435
20°	0.12748	0.78473	1.363	0.01703	0.79007	1.798
25°	0.17458	0.79345	0.754	0.02182	0.77285	1.321
30°	0.25418	0.7867	0.714	0.0299	0.7403	1.265

It should be noted that the constants in Table 3.1 are valid only for channel pitch length of 0.0246 m and hydraulic diameter D_h, of 0.00122 m. Also, the Hesselgreaves correlations

used herein are only valid for constant surface heat flux conditions.

Based on the Nusselt numbers calculated for the hot and cold side, the corresponding convective heat transfer coefficients were calculated using the following relationship

$$Nu = \frac{hD_h}{k_f} \tag{3.18}$$

Here, h is the convective heat transfer coefficient and k_f is the thermal conductivity of the fluid.

As mentioned earlier, the thermal conductance, which is a product of the overall heat transfer coefficient and the heat transfer area, is related to the heat transfer mechanisms in the HX, which include convection from the hot fluid to the wall of the HX, conduction through the wall, and from the wall to the cold fluid via convection. The convective heat transfer coefficients and the conduction through the wall can be related to the thermal conductance as follows

$$\frac{1}{UA} = \left[\frac{1}{h_h A_h} + \frac{t_e}{k_w A_w} + \frac{1}{h_c A_c}\right] \tag{3.19}$$

Here, A_h and A_c represent the convective heat transfer areas of the hot and cold sides, and A_w refers to the conductive heat transfer area between the plates. Also, t_e is effective thickness of the wall and k_w is the thermal conductivity of the wall material. The effective thickness was calculated by setting the area of the cross hashed rectangle, highlighted in in Figure 3.1 by dark gray, equal to half the area under the cold channel, depicted by the light gray hashed zone. This when simplified results in

$$t_e = t_p - \pi\frac{d_c}{8} \tag{3.20}$$

where d_c is the channel diameter and t_p is the plate thickness.

In order to calculate A_w, the effective width, w_e, of the heat transfer area between the channels in a single heat transfer unit cell, as shown in Figure 3.2, was calculated,

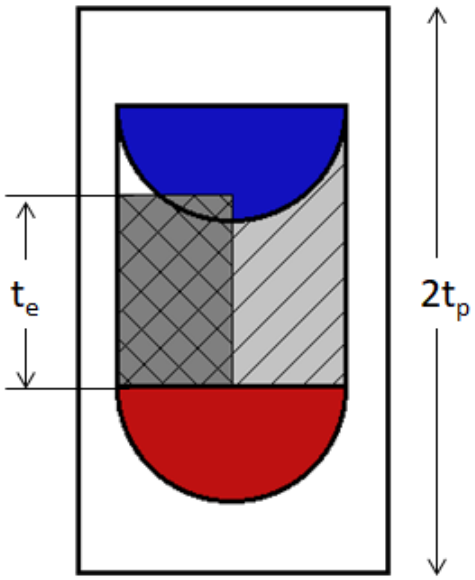

Figure 3.1: Schematic of effective thickness of conduction zone in PCHEs

and then was multiplied by the number of hot or cold channels in the HX design. The effective width was acquired by setting the shaded area in Figure 3.2 equal to product of effective thickness and the effective width.

This was simplified to

$$w_e = \frac{d_c t_p - \frac{\pi}{8} {d_c}^2}{t_e} \tag{3.21}$$

Equation 3.19 can be simplified by assuming that the convective heat transfer areas on the hot and cold sides are exactly equal to the total heat transfer area A. The simplification results in

$$\frac{1}{U} = \left[\frac{1}{h_h} + \frac{t_e}{k_w} \frac{A}{A_w} + \frac{1}{h_c} \right] \tag{3.22}$$

Once U was calculated, the area of heat transfer was acquired by rearranging terms in Equation 3.11. Using the heat transfer area, the channel lengths were calculated using the following relationship

$$L_{ch} = \frac{A}{N_c P_c} \tag{3.23}$$

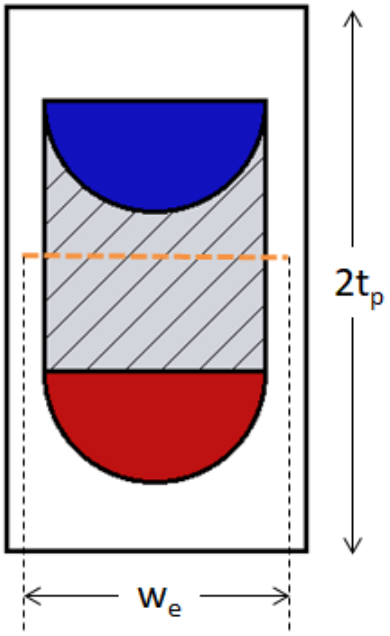

Figure 3.2: Schematic of effective width of conduction zone in PCHEs

where N_c represents the total number of channels, P_c refers to the perimeter of a single channel and L_{ch} was the calculated HX channel length. Using the channel length, the pressure drops along the channels was calculated using the Darcy-Weisbach equation given as

$$\Delta P = 4f\frac{L_{ch}}{D_h}\frac{1}{2}\rho v^2 \tag{3.24}$$

where ρ is the average fluid density and v, the mean fluid velocity. Using the mass flow rates of the hot and cold fluids, their average densities and their overall pressure drops, the pumping power, $\dot{W}$, required to operate the PCHEs was calculated as follows

$$\dot{W} = \frac{\dot{m}\Delta P}{\rho} \tag{3.25}$$

The maximum pumping power requirement, from between the hot and cold streams, was later used for calculating the operational cost for the HX system.

It should be noted that the channel length for zigzag PCHEs is larger than the actual

length of the HX (see Figure 3.3). In order to acquire the length of the HX, the channel length was multiplied by the cosine of the pitch angle.

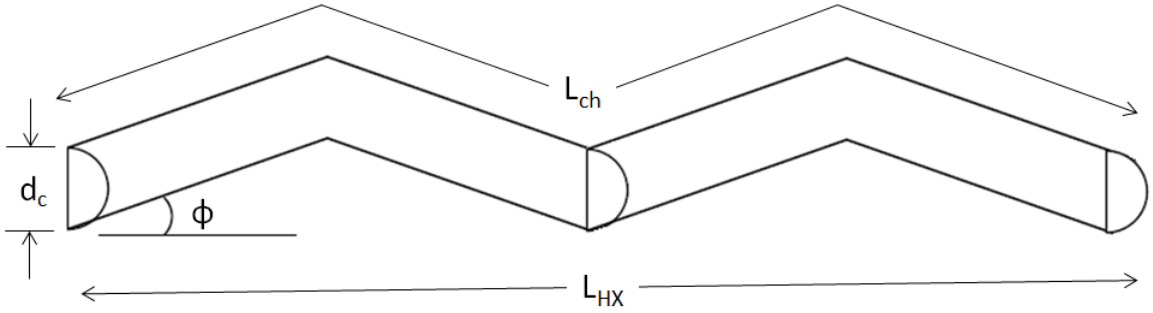

Figure 3.3: Channel length vs. HX length in zigzag PCHEs

This concluded the thermal hydraulic calculations that were required to acquire the total number and lengths of channels in the PCHE designs, which would satisfy all of the boundary conditions. In order to calculate the volumes of the PCHEs, the following steps were carried out.

- For a fixed width of 0.6 m and a channel pitch of 0.0025 m, the maximum number of channels that could fit within a single plate for straight PCHEs was calculated to be 240, and that for a zigzag PCHEs with a pitch angle of 30° was calculated to be about 235. For the sake of consistency, all PCHE zigzag designs were assigned a maximum number of channels per plate as 235.
- In the case of zigzag PCHEs, the length of the HX was calculated from the length of the channel, by taking into account the cosine of the pitch angle.
- The total number of plates, either for the hot or the cold fluid side, was acquired by dividing the total number of channels by the maximum number of channels per plate. This number was then doubled to get the total number of HX plates in the design.
- Based off the total number of plates in the HX and plate thickness, the total height of the HX was acquired.

- Using the calculated length of the HX, the height and the allowed width, the volume of the PCHEs were acquired.

The solution methodology followed for the PCHE sizing calculations can be depicted by a simplified flowchart given in Figure 3.4.

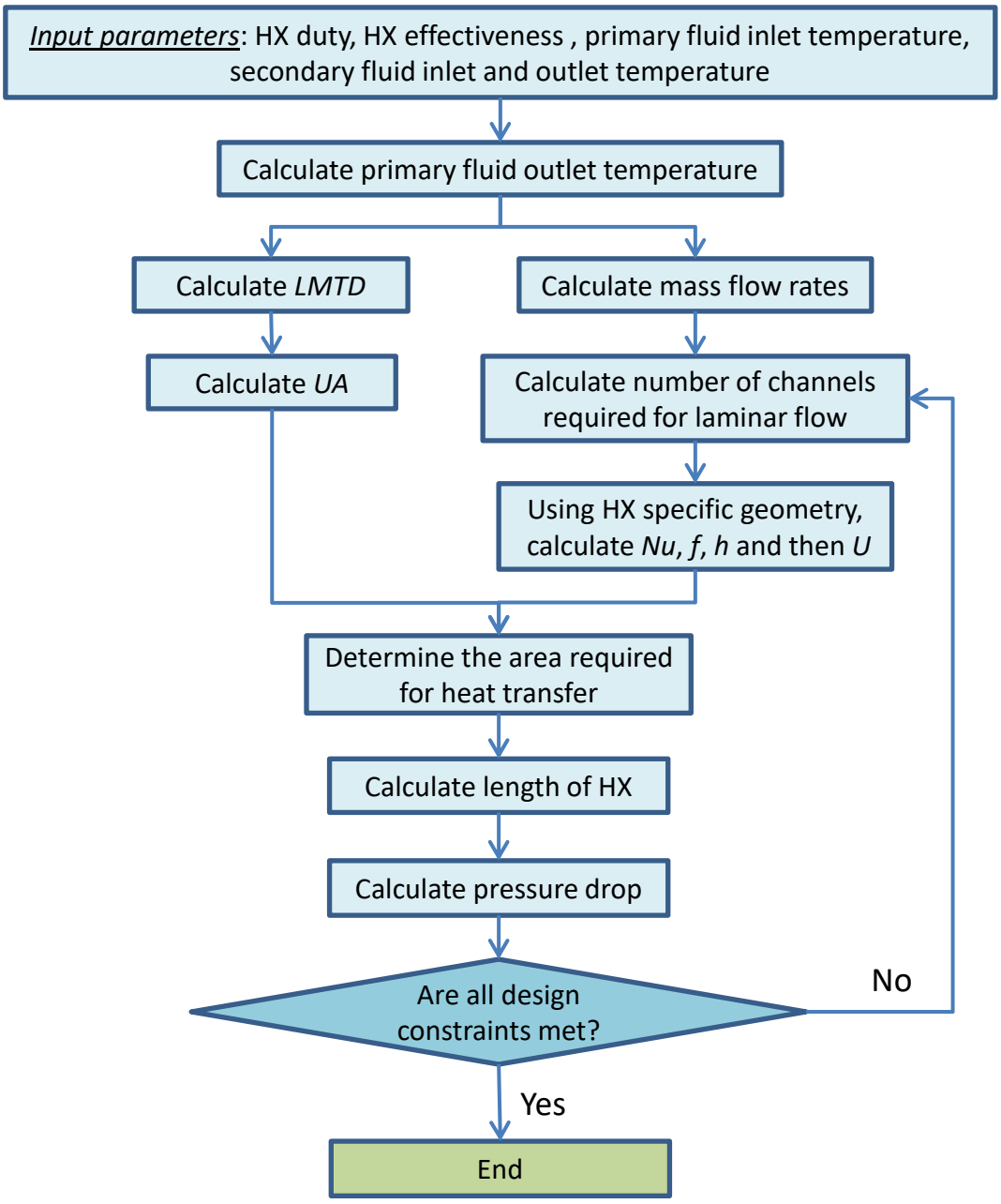

Figure 3.4: Solution methodology for PCHE sizing

3.2 Calculations for HCHE

Similar to the calculations performed for the PCHEs, the first step in the HCHE sizing calculations was to acquire the hydraulic diameter. As the geometry is that of a tube-in-tube annular design, the hydraulic diameter simplifies to

$$D_h = d_{o,i} - d_{i,o} \tag{3.26}$$

where $d_{o,i}$ and $d_{i,o}$ are the inner diameter of the outer tube, and outer diameter of the inner tube, respectively.

In the case of HCHE hydrodynamic calculations, the only constraint of concern was that of the allowable pressure drop in the system. Thus, using a similar methodology followed in section 3.1, HCHE sizing calculations were performed. Herein, the number of tubes was varied till the pressure drop constraint was met, and then calculations for Reynolds number and the overall heat transfer coefficient were performed. Once U was calculated, the heat transfer area was acquired, and therefore the length of the tubes.

The heat transfer correlations for tube-in-tube HCHE were acquired from the Heat Exchanger Design Handbook [29]. For laminar flow (Re < 2300), the Nusselt number, Nu, was calculated using Schmidt's equation

$$Nu_l = 3.65 + 0.08 \left[1 + 0.8 \left(\frac{D_h}{D_c} \right)^{0.9} \right] Re^m Pr^{1/3} \left(\frac{Pr}{Pr_w} \right)^{0.14} \tag{3.27}$$

where

$$m = 0.5 + 0.2903 \left(\frac{D_h}{D_c} \right)^{0.194} \tag{3.28}$$

Here, D_c here is the coil diameter, also known as diameter of curvature, Pr is the Prandtl number at mean fluid temperature and Pr_w is the Prandtl number at the wall temperature. However, as the wall temperatures were not available for this analysis, Pr_w was calculated

at the inlet temperatures of the hot and cold fluids. It should be noted that the hydraulic diameters would be different for the hot and cold fluid streams, as the hot fluid flows within the inner tube and the cold fluid flows through the annulus.

The Nusselt number for transitional flow, where $\mathrm{Re}_{crit} < \mathrm{Re} < 2.2 \text{ x } 10^4$, is given by

$$Nu_{tr} = ANu_{l,Re_{crit}} + (1 - A)Nu_{t,Re_t} \tag{3.29}$$

Here

$$A = \frac{2.2 \times 10^4 - Re}{2.2 \times 10^4 - Re_{crit}} \tag{3.30}$$

and $Nu_{l,Re_{crit}}$ refers to the laminar Nusselt number calculated with Re_{crit}, and Nu_{t,Re_t} refers to the turbulent flow Nusselt number calculated with Re_t as Reynolds number. Re_{crit} is the critical Reynolds number and Re_t is the point at which transitional flow ends. These Reynolds numbers are given as follows

$$Re_{crit} = 2300 \left[1 + 8.6 \left(\frac{D_h}{D_c}\right)^{0.45}\right] \tag{3.31}$$

and

$$Re_t = 22000 \tag{3.32}$$

For fully developed turbulent flow at $\mathrm{Re} > 2.2 \text{ x } 10^4$, the Nusselt number proposed by Gnielinski is given by

$$Nu_t = \frac{(f_t/8)RePr}{1 + 12.7\sqrt{f_t/8}(Pr^{2/3} - 1)} \left(\frac{Pr}{Pr_w}\right)^{0.14} \tag{3.33}$$

where the turbulent Fanning friction factor, f_t, is proposed by Mishra and Gupta, and is given by,

$$f_t = \left[\frac{0.3164}{Re^{0.25}} + 0.03\left(\frac{D_h}{D_c}\right)^{0.5}\right]\left(\frac{\eta_w}{\eta}\right)^{0.27} \tag{3.34}$$

Here, η_w is the dynamic viscosity at the wall temperature, but for the purposes of this analysis, it was calculated at the inlet temperatures. Using the Nusselt numbers, the calculations for convective heat transfer coefficients were performed similar to that of the PCHEs.

The relationship between the thermal conductance, the convective heat transfer coefficients and the conduction through the annular geometry in the HCHE tubes can be given by

$$\frac{1}{UA} = \left[\frac{1}{h_h A_h} + \frac{ln(d_{i,o}/d_{i,i})}{2\pi k_w} + \frac{1}{h_c A_c}\right] \tag{3.35}$$

where

$$\frac{ln(d_{i,o}/d_{i,i})}{2\pi k_w} \tag{3.36}$$

is the radial thermal resistance in an annular geometry. As the definition of the product UA is arbitrary, the correlation was simplified by factoring out the inner most area of heat transfer. This simplified the correlation to

$$\frac{1}{UA} = \left[\frac{1}{h_h} + d_{i,i}\frac{ln(d_{i,o}/d_{i,i})}{2\pi k_w} + \left(\frac{d_{i,i}}{d_{i,o}}\right)\frac{1}{h_c A_c}\right] \tag{3.37}$$

Using Equation 3.37, the area of heat transfer was calculated. Following this, the length of the HX tubes, the pressure drops across HX designs, and therefore, the pumping power required, were calculated using methodology similar to that for the PCHEs.

CHAPTER 4

Results and Analysis

Chapter 4 presents the results of the mathematical modeling and calculations performed, as mentioned in Chapters 2 and 3, and then proceeds with the analysis of the data acquired. Section 4.1 provides numerical and visual data with the help of tables and plots, displaying the key relationships between different parameters and highlighting the important results. Section 4.2 analyzes the data acquired by taking into account the design constraints and the HX performance parameters. Section 4.3 then presents a single case for the uncertainty analysis that was performed for the different HX designs.

4.1 Heat Exchanger Performance

The results of the sizing calculations performed for the different HXs, taking into account the different fluid sets, their operating conditions and design constraints, are presented in Table 4.1. The first column lists the fluid sets that were chosen in this study, and columns 2 - 8 represent the volumes of the PCHEs. The pitch angle 0° corresponds to the straight PCHE, and the incremental values thereafter to 30° are the zigzag designs. The last column in the table presents data for the HCHE volumes.

Table 4.1: Heat exchanger volumes based on sizing calculations (m^3)

Fluid Sets	PCHE							HCHE
	0°	5°	10°	15°	20°	25°	30°	
He-He	49.7	28.2	23.0	20.7	19.2	18.2	17.5	262.0
He-SCO_2	148.8	86.9	71.4	64.2	56.6	51.2	47.0	388.2
FLiNaK-He	39.6	34.3	30.9	28.5	26.0	24.2	22.6	480.1
FLiNaK-SCO_2	146.2	88.8	70.1	63.7	56.7	51.6	47.7	617.3
$KFZrF_4$-He	57.5	44.2	38.2	35.0	31.7	29.7	27.9	479.8
$KFZrF_4$-SCO_2	164.0	101.2	84.7	76.8	68.2	62.1	57.1	641.0

It is evident from the tabulated values that with an increase in pitch angle, the volume of the HXs decreases, with volume reduction by nearly a factor of 3 when going from

PCHE straight to PCHE zigzag with a pitch angle of 30°. It can also be seen that the volume of the HCHEs is significantly larger for every fluid set studied, by a factor ranging from 2, when compared to PCHE straight, to 5, when compared to the PCHE zigzag designs with a pitch angle of 30°. The data presented in Table 4.1 for the PCHEs can be better visualized with plots provided in Figure 4.1.

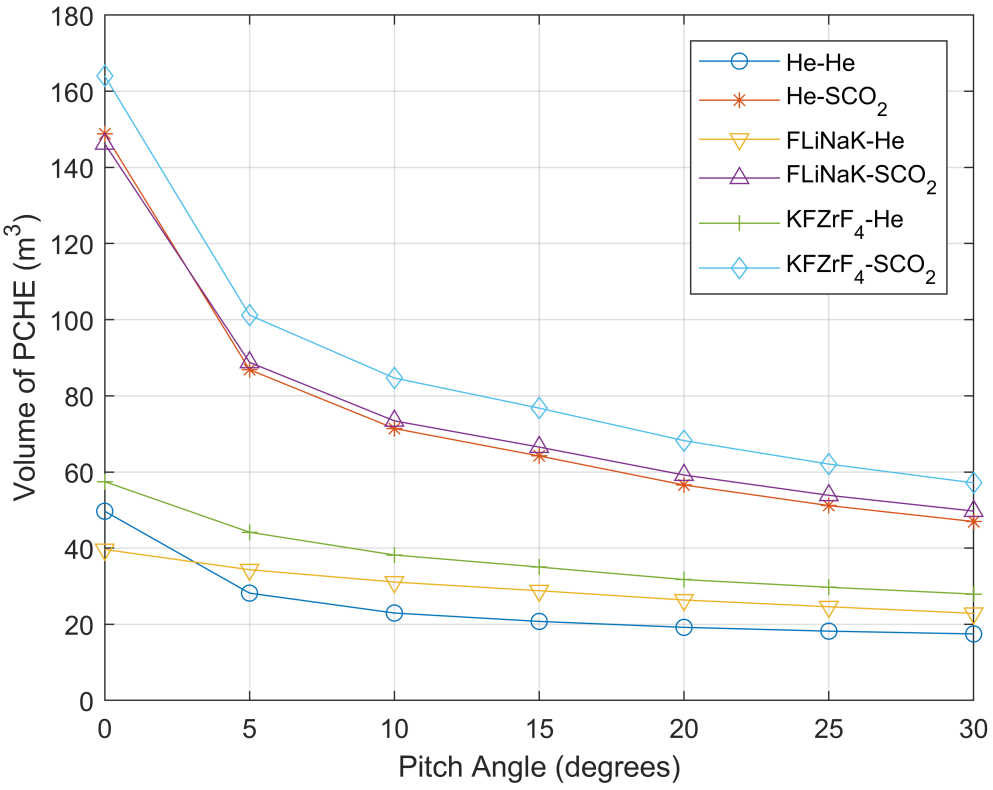

Figure 4.1: Effect of pitch angle on PCHE volumes

Here, the x-axis represents the pitch angles that were varied for the PCHEs and the y-axis represents their respective calculated volumes. It can be seen from the figure that the changes in volumes for HXs follow the same pattern for all the fluid sets, when the pitch angle is increased. The plots depict the significant drop in HX volumes when moving from straight PCHEs to zigzag channeled designs. This is a result of the decrease in the amount of HX surface area that is required to transfer the heat.

The heat transfer area required for each HX design is plotted in Figure 4.2. It can be seen that the plots for HX volumes and those for HX heat transfer areas follow the same exact pattern. This is due to the fact that the width of the HX plate is fixed to 0.6 m, thus allowing the comparison of the 3-dimensional volume to the 2-dimensional heat transfer area.

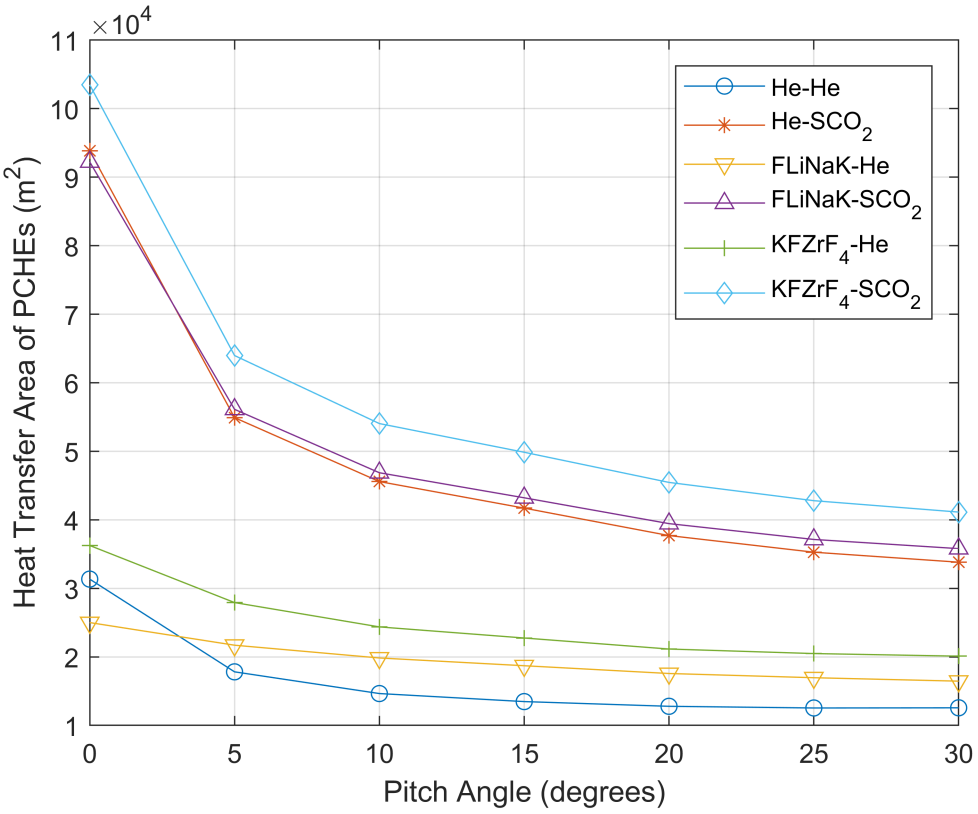

Figure 4.2: Effect of pitch angle on PCHE heat transfer areas

Based on the thermal hydraulic performance of the HXs, two FOMs were developed as mentioned in Section 2.2. FOM_1, which is the ratio of the overall heat transfer coefficient to the overall pressure drop, was chosen as a metric for comparison because it indicates the maximum thermal performance that can be achieved for the minimum pressure drop in the HX. The calculated values for FOM_1 are provided in Table 4.2, and the plots of the same can be seen in Figure 4.3.

Table 4.2: Developed FOM_1 values from thermal hydraulic calculations (W/m^2K-kPa)

Fluid Sets	PCHE							HCHE
	0°	5°	10°	15°	20°	25°	30°	
He-He	29.4	36.4	38.8	33.9	29.2	24.1	19.6	11.9
He-SCO_2	29.5	60.9	74.5	73.5	72.7	67.8	59.6	7.9
FLiNaK-He	296.3	283.1	253.7	219.8	189.0	159.8	136.8	58.5
FLiNaK-SCO_2	203.0	333.6	419.6	481.0	429.4	356.8	290.6	76.1
$KFZrF_4$-He	37.4	39.8	41.4	41.6	42.3	41.2	40.5	80.7
$KFZrF_4$-SCO_2	277.4	387.9	390.7	338.7	297.0	246.7	202.6	12.5

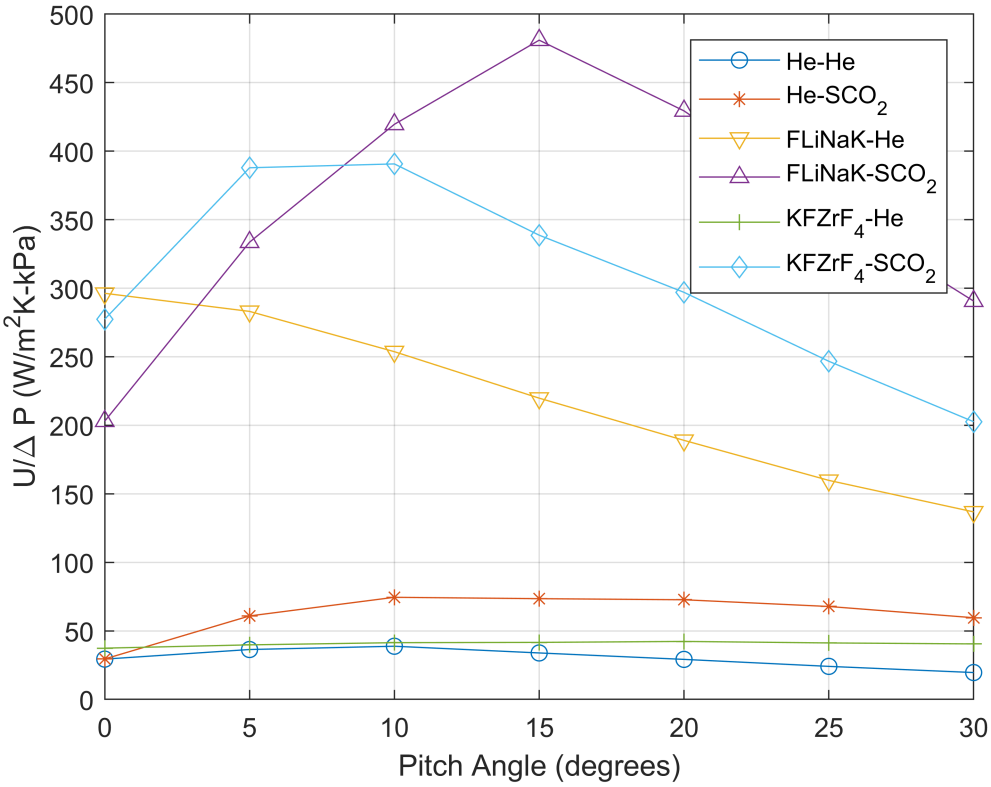

Figure 4.3: Effect of pitch angle on FOM_1 values for PCHEs

The primary y-axis in Figure 4.3 represents the FOM_1 values whereas the x-axis represents the incremental pitch angles of the various PCHEs. The FOM_1 plots display a pattern that indicates the fact that for a combination of a particular fluid set, operating conditions and design constraints, there exists an optimum design, indicated by peak points on the plots, that would result in the highest heat transfer possible for the lowest

pressure drop. For example, referring to the fluid set of FLiNaK-SCO_2, the peak occurs at 15°, corresponding to a PCHE zigzag design, whereas that for FLiNaK-Helium, the peak occurs at 0°, corresponding to a straight PCHE.

FOM_2, which is the ratio of overall pressure drop to the length of the HX channel is a metric that was used to compare various PCHE designs. As the channel cross sectional dimensions for the PCHEs are the same but the lengths are different, FOM_2 allows to see the effect of changes in pitch angle on the pressure drop in the HX. It is also an indicator of the fact that a decrease in HX length comes with a penalty of an increase in pressure drop. The calculated values for FOM_2 are provided in Table 4.3, and the plots of the same can be seen in Figure 4.4.

Table 4.3: Developed FOM_2 values from thermal hydraulic calculations (kPa/m)

Fluid Sets	PCHE							HCHE
	0°	5°	10°	15°	20°	25°	30°	
He-He	12.5	18.7	26.0	35.2	50.3	70.5	95.5	4.5
He-SCO_2	4.2	5.3	6.3	7.6	9.4	11.5	14.2	3.5
FLiNaK-He	5.7	7.4	9.6	12.4	16.2	20.5	25.6	0.5
FLiNaK-SCO_2	1.2	1.5	1.7	1.7	2.3	3.2	4.2	0.3
$KFZrF_4$-He	11.1	16.6	21.3	25.8	31.3	36.6	41.7	0.4
$KFZrF_4$-SCO_2	0.5	0.9	1.2	1.7	2.3	3.2	4.2	3.4

As expected, the values for FOM_2 as provided in Table 4.3 and Figure 4.4 increase with an increase in pitch angle of the PCHEs for all fluid sets. This is a result of the additional frictional pressure drop that arises due to zigzag pattern of the fluid channels.

4.2 Design Analysis

The plots presented in Section 4.1 have provided quantitative parameters to compare the various types of PCHEs for the different fluid sets that have been considered for this study. The decrease in HX volumes for the PCHEs with the increase of pitch angles can be attributed to an increase in heat transfer coefficients of the fluid streams. The

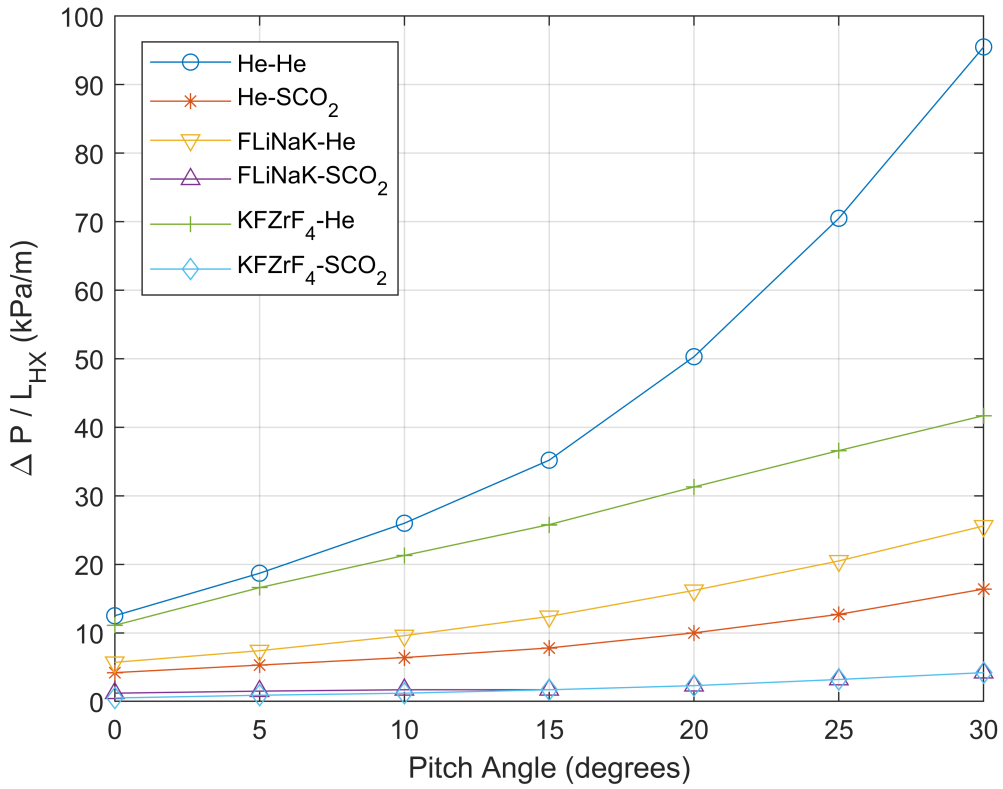

Figure 4.4: Effect of pitch angle on FOM_2 values for PCHEs

zigzag pattern causes the fluid particles to mix, thus disrupting the boundary layer of an otherwise fully developed laminar flow. Higher the pitch angle, more the mixing of fluid and therefore higher the disturbance caused in the flow. This enhanced mixing increases the Nusselt number, leading to higher convective heat transfer coefficients of the fluid streams. With an increase in the convective heat transfer coefficients, the overall heat transfer coefficient also increases. Now, as the product UA is independent of the HX geometry for the same given duty and temperature conditions, the increase in overall heat transfer coefficient is compensated for by a decrease in the total heat transfer area. This is supported by the plots in Figure 4.2.

Figure 4.1 also shows that the HXs with Helium as their secondary fluid have considerably smaller volumes when compared to those containing SCO_2. This can be attributed

to the fact that SCO_2 has a lower thermal conductivity and lower heat capacity, causing the HX to require more surface area, to transfer the same amount of heat as that of a HX with Helium. This is also supported by Figure 4.2. In other terms, smaller HX volumes for systems with Helium as their secondary working fluid can be attributed to the fluid's higher thermal conductivity and heat capacity.

In trying to understand the effect of pitch angles on the thermal hydraulic performance of the HXs, it can be see from Figure 4.3, that increments in pitch angles favors heat transfer for all the fluid sets studied except for FLiNaK-Helium. The most significant effects can be seen in the cases of HX designs that involve heat transfer between molten salts and gas, particularly SCO_2. As mentioned earlier, with an increase in pitch angle, there is an increase in the overall heat transfer coefficient. This rise is fairly significant when moving from a straight channeled PCHE to a zigzag design, and gradually starts to plateau between 15° to 30°. In contrast to this, the frictional pressure drop increases exponentially when moving from the straight to the zigzag design with 30° pitch angle. The nature of these increments, in the overall heat transfer coefficient and pressure drops, leads to their ratios being larger for certain pitch angles. This results in the peaks of FOM_1 which can be seen in Figure 4.3. It should be noted that this is true for all fluid sets except FLiNaK-Helium. For FLiNaK-Helium, the increments in overall heat transfer coefficients are far less drastic when compared to the pressure drops. This results in ratios of FOM_1 parameters to decrease as and when the pitch angle is increased, and thus the plot has a declining trend.

In the case of FOM_2, an increase in pitch angle does increase the friction factors and therefore the overall pressure drops, but this is counteracted by a decrease in the length of the PCHE channels in order to limit the pressure drop below 1% of the operating pressure. This decrease in length, causes the PCHEs to perform near the upper limit of the allowable pressure drop and also results in the incremental behavior in FOM_2 values.

The decrease in lengths of the HXs with respect to changes in the pitch angles is provided in Table 4.4 and can be seen with the help of Figure 4.5.

Table 4.4: Heat exchanger channel lengths based on sizing calculations (m)

Fluid Sets	PCHE							HCHE
	0°	5°	10°	15°	20°	25°	30°	
He-He	1.50	1.42	1.17	1.07	0.92	0.81	0.73	15.39
He-SCO_2	1.50	0.97	0.80	0.72	0.63	0.57	0.52	19.78
FLiNaK-He	0.45	0.42	0.39	0.38	0.36	0.35	0.33	16.23
FLiNaK-SCO_2	0.86	0.67	0.60	0.55	0.50	0.47	0.46	19.05
$KFZrF_4$-He	1.27	1.03	0.88	0.78	0.68	0.61	0.56	14.45
$KFZrF_4$-SCO_2	1.31	0.85	0.72	0.66	0.61	0.57	0.55	17.38

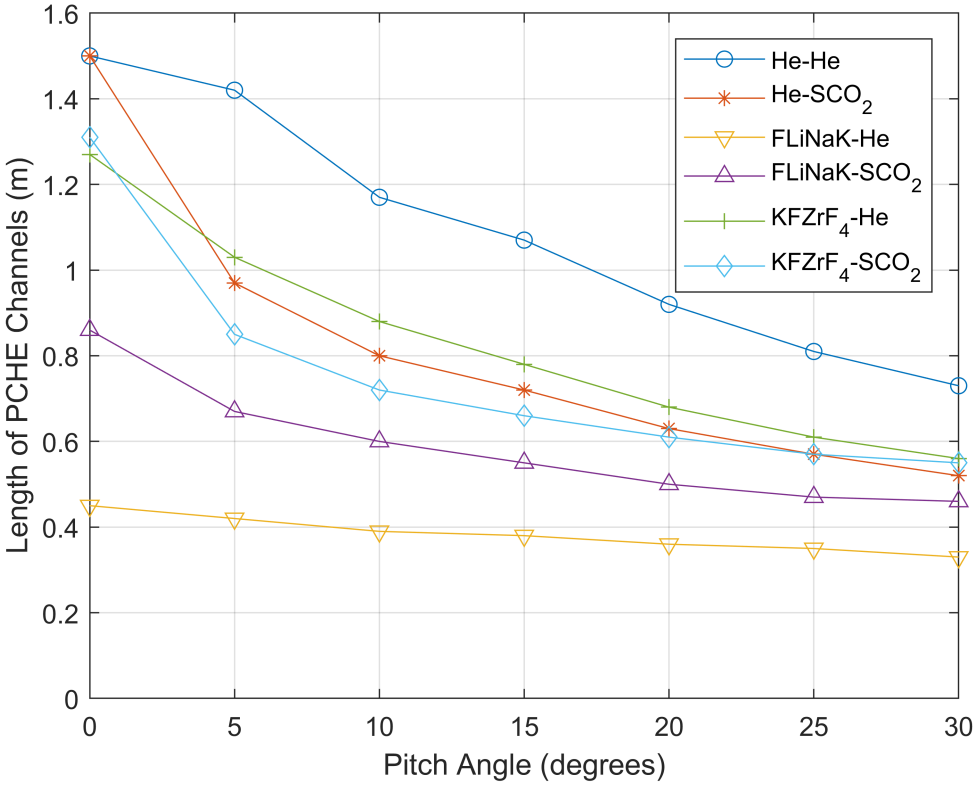

Figure 4.5: Effect of pitch angle on PCHE channel lengths

From the figures for FOM_1 and FOM_2, it is clear that although increasing the pitch angle improves the thermal performance of the HXs, it comes with a penalty of a higher

pressure drops. This needs to be taken into account during the overall optimization and economic analysis of the heat transfer systems.

Based on the geometric limitations of the HX plate dimensions due to current manufacturing capabilities, single HX units for the calculated volumes of the PCHEs, as provided in Table 4.1, would result in unreasonably tall HXs. This begs the need of having smaller HX modules that would be connected in parallel to transfer the required heat. For the purposes of this study, the total height of the stacked plates, and therefore the PCHEs was set to 3 m. This limited the maximum volume of a single PCHE module to 2.7 m^3. A single PCHE module could be represented by a cuboid, the schematic of which is provided in Figure 4.6. Here L_{HX} is the calculated HX length, along the flow direction.

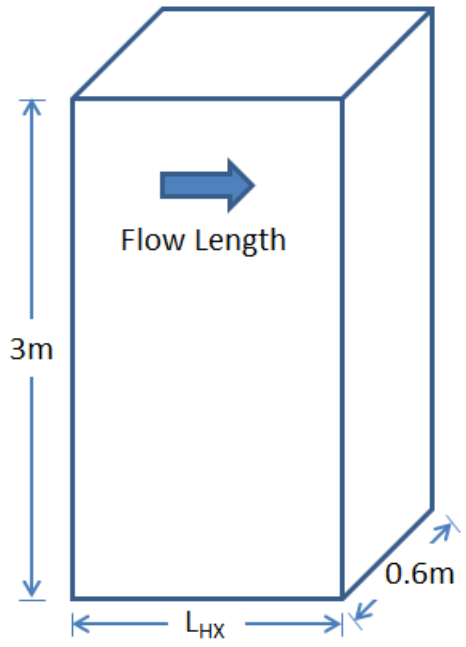

Figure 4.6: Schematic of single PCHE module

Another metric used to compare the thermal hydraulic performance of the HXs is compactness, which is a ratio of the heat transfer surface area of the HX to its volume. By definition, compact HXs are supposed to have higher compactness when compared

to conventional HXs. This is achieved via higher heat transfer coefficients that generate from the distinctive surface geometries of the compact HXs. The relationship between pitch angle increments in PCHEs and compactness is shown in Figure 4.7.

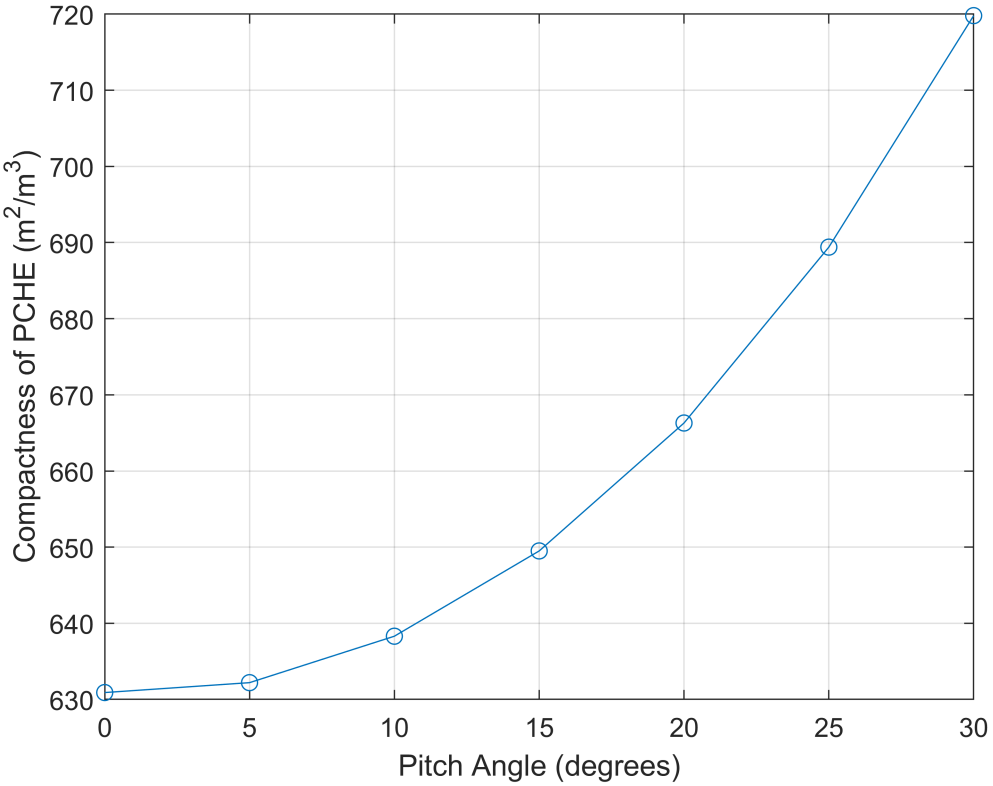

Figure 4.7: Effect of pitch angle on PCHE compactness

This plot shows that in going from straight to zigzag PCHE with a pitch angle of 30°, the compactness of the HX increases by about 15%. Higher compactness indicates that the HX can be smaller in design. The compactness ($\bar{C}$) data for PCHEs provided in Figure 4.7 was curve fit, resulting in an equation as a function of pitch angle given by

$$\bar{C}(\phi) = 0.115\phi^2 - 0.524\phi + 631.4 \tag{4.1}$$

This can be used to estimate PCHE compactnesses at various pitch angles. In comparison to the compactness for PCHEs, the HCHE compactness is merely 78 m^2/m^3.

4.3 Uncertainty Analysis

Some of the correlations, used for the sizing and thermal hydraulic calculations performed, have uncertainties associated with them. These were taken into account while conducting the sizing process. However, the preliminary results that were acquired from the uncertainty analyses suggested that the propagation of these errors would not affect the final results of HX volumes or costs significantly. To support this fact, the uncertainty analysis results for the Helium-Helium heat transfer case are provided below.

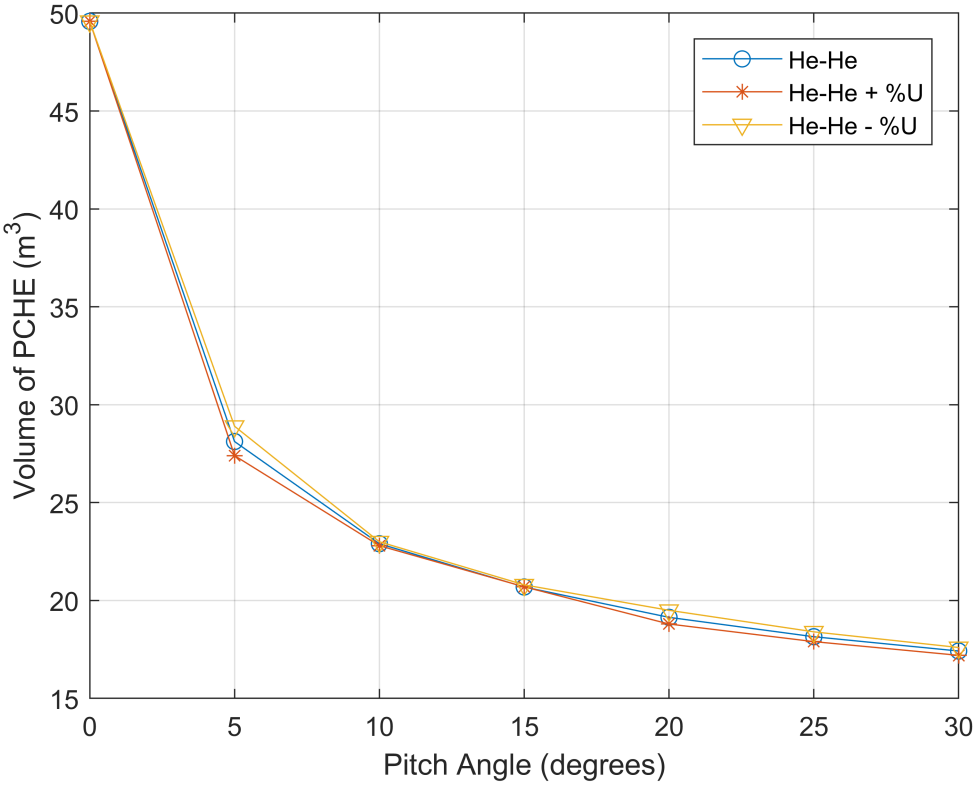

Figure 4.8: Uncertainties in PCHE volumes for Helium-Helium

Figure 4.8 displays the uncertainties ($\%U$) in the HX volumes for the Helium-Helium heat transfer case. These uncertainties are based off the RMSE values provided in Table 3.1 for both, the Fanning friction fact and the Nusselt number. Similarly, uncertainty

analyses were carried out for the two developed FOMs, the plots of which are provided in Figures 4.9 and Figure 4.10. The effect of the uncertainty propagation resulted in variance of HX costs by less than 1% in the case of PCHEs.

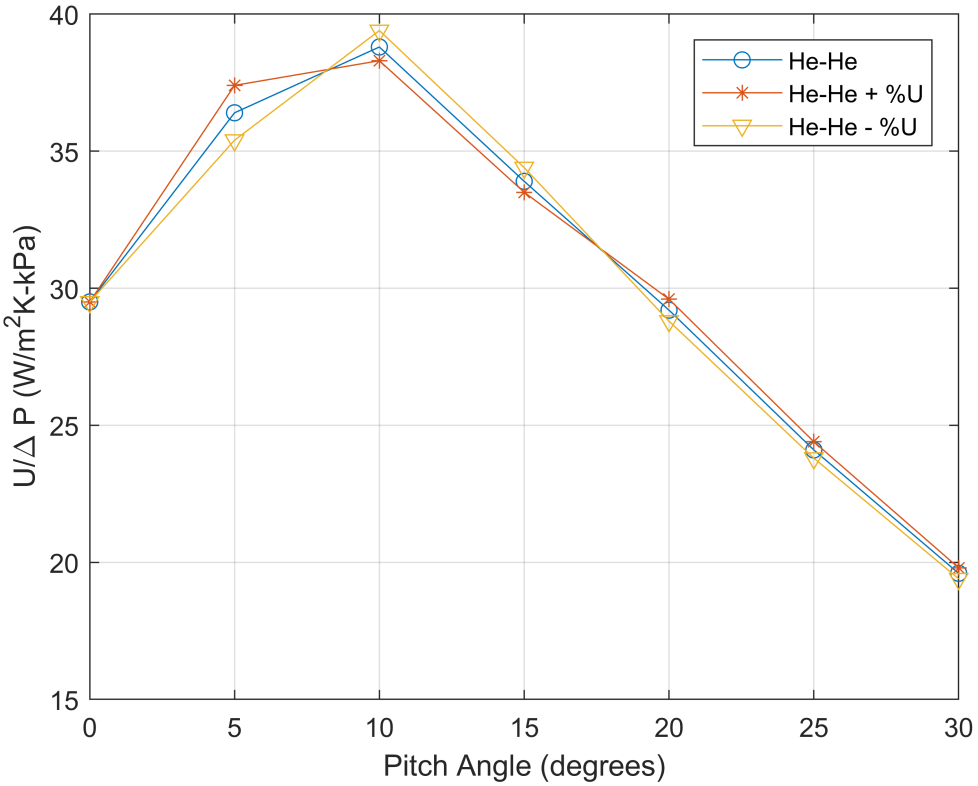

Figure 4.9: Uncertainties in FOM_1 values for Helium-Helium in PCHEs

For HCHEs, the sources for uncertainties were the correlations wherein the assumption was made to use the inlet temperatures, instead of the wall temperatures to calculate the Prandtl numbers and the dynamic viscosities for the various fluid sets. In order to analyze the effects caused by this assumption, calculations for the Prandtl number and dynamic viscosities were made using the average temperature and the outlet temperature, and the results of this analyses were compared to the results acquired from the previous assumption. In the case of the HX lengths, the changes in temperature assumptions led to variances of less than 1%, and for the total HX costs, the variances were less that 0.5%.

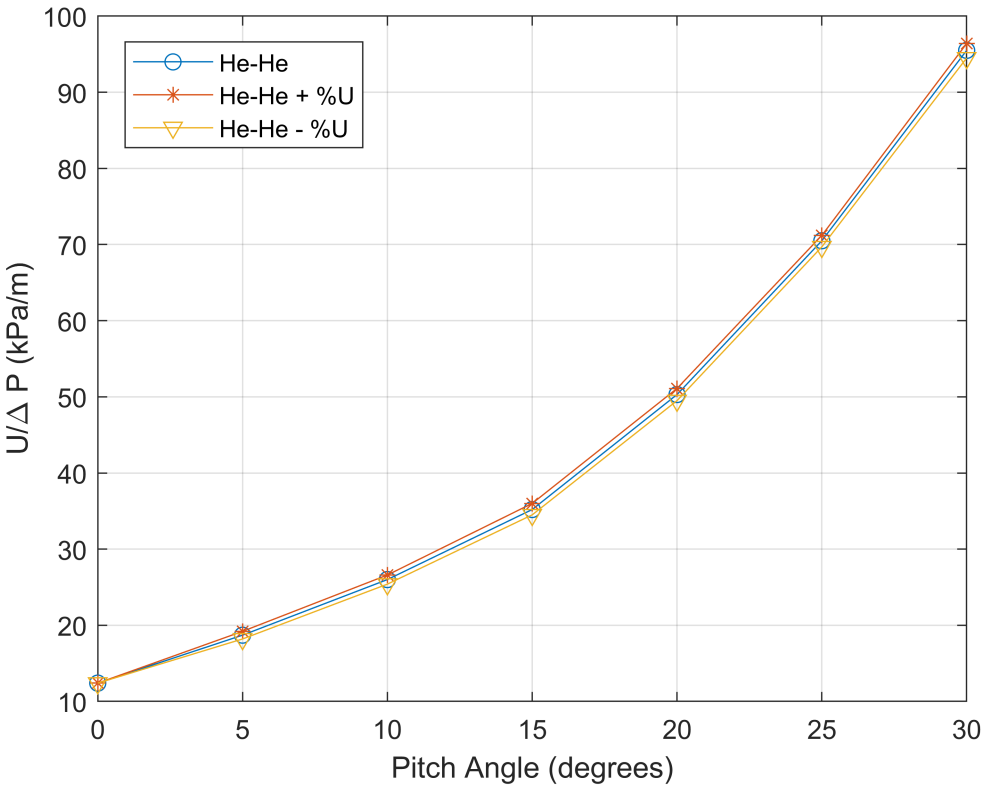

Figure 4.10: Uncertainties in FOM_2 values for Helium-Helium in PCHEs

Thus the uncertainty propagations were ignored while performing further calculations for all the HX designs.

CHAPTER 5

Heat Exchanger Costing

Chapter 5 describes the preliminary cost analysis that was performed for the various HX designs, based on the results of their sizing and thermal hydraulic performances. The total cost was assumed to be the sum of the capital cost and the operating cost of the HXs, over an assumed operational lifetime of 10 years. Sections 5.1 and 5.2 provide a brief overview of how the capital costs and operating costs were calculated.

5.1 Capital Cost

For the purposes of this study, the capital cost included only the cost of the material required for the construction of the HXs. An assumption made by Heatric was that if the HXs used in nuclear applications were made of stainless steel, the cost for material used would be roughly around \$30/kg [12], [27]. In the event that stainless steel could not be used for the specific operating conditions, titanium would be used instead. This however would cost 4 times as much as stainless steel. For this study, Alloy 617 was assumed to cost similar to titanium and thus using the information provided by Heatric, a price of \$120/kg was used. The capital cost was assumed to be a fixed cost as it is a one-time investment, the calculations for which are described as follows

- For PCHEs, the total volume of the flow channels was calculated knowing their cross sectional areas and lengths. This being the void volume in the PCHEs when not in operation, was subtracted from the total volume of the HXs, thus resulting in the volume of only the material required for the construction of the HXs.
- For HCHEs, the volumes of the material required was calculated based off the thickness of the helically coiled tubes and their lengths.
- The mass of the material required for the HXs was calculated using the material

volume and density of Alloy 617.

- The capital cost was then calculated by multiplying the mass of the material by assumed cost/kg of the material.

5.2 Operational Cost

The operational cost for the HXs was calculated based off the pumping power that would be required to overcome the pressure drops in the system, and the cost of electricity required to operate the pump. For the following calculations, the national average retail cost of electricity of 12 ¢/kWh was used [14].

- The total number of operational hours were calculated based off the assumed operational life of the HXs of 10 years, at 100% capacity.
- The pumping power calculated by using Equation 3.25 was multiplied by the total number of operational hours for the HXs.
- The number of hours was then multiplied by the retail cost of electricity to get the total operational cost.

The total costs for the various fluid sets, which represent the sum of the capital as well as the operational costs, are provided in Table 5.1 and plotted in the sub-figures of Figure 5.1. The stacked bar plots combine the capital and operational cost into the total cost, represented by the total height of the bars for the different HX configurations labeled on the x-axis. The y-axis represents the total cost of the HX systems, operating for 10 years, in millions of USD.

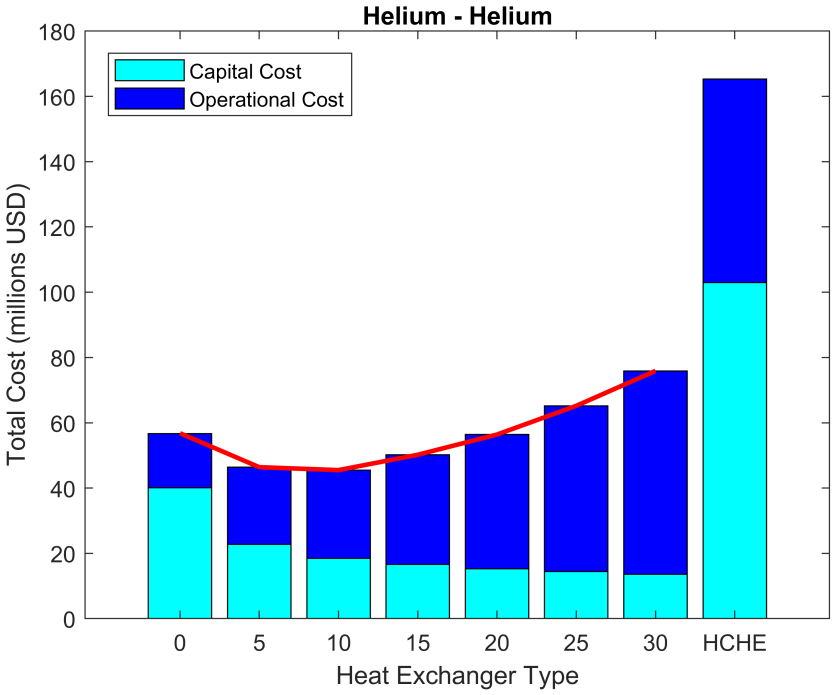
Helium - Helium
Capital Cost
Operational Cost
Total Cost (millions USD)
0
20
40
60
80
100
120
140
160
180
0
5
10
15
20
25
30
HCHE
Heat Exchanger Type

(a)

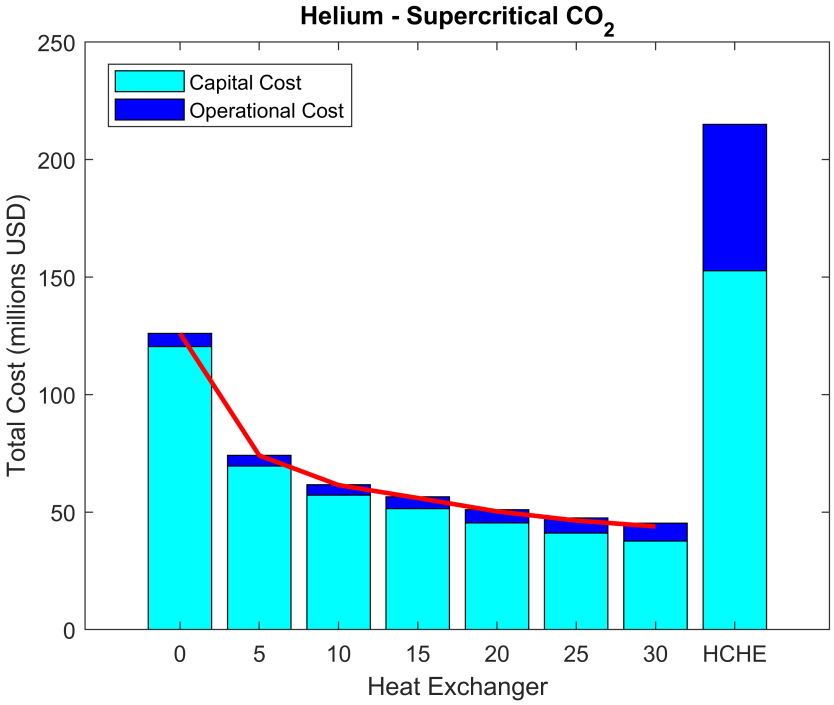
Helium - Supercritical CO2
Capital Cost
Operational Cost
Total Cost (millions USD)
0
50
100
150
200
250
0
5
10
15
20
25
30
HCHE
Heat Exchanger

(b)

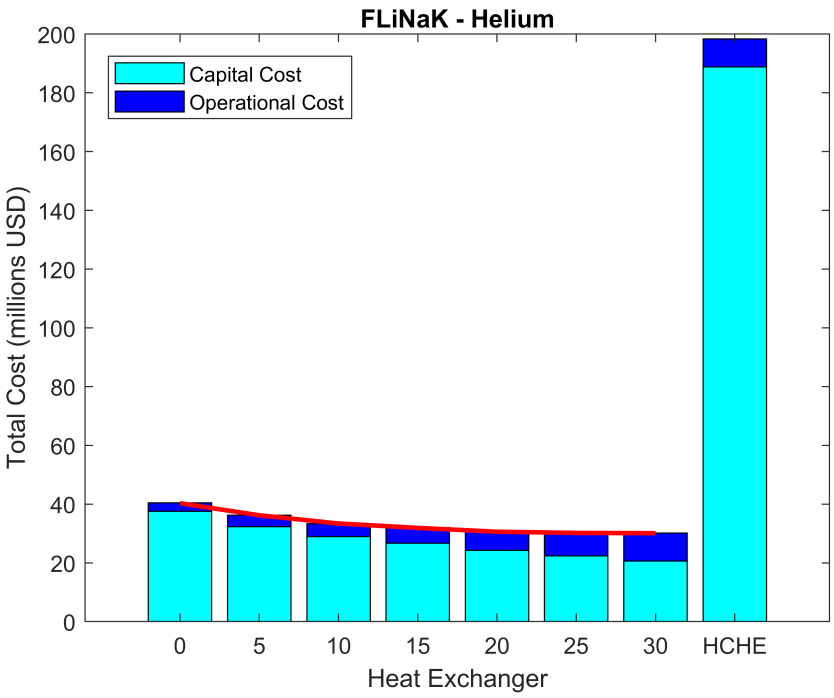
FLiNaK - Helium
Capital Cost
Operational Cost
Total Cost (millions USD)
0
20
40
60
80
100
120
140
160
180
200
0
5
10
15
20
25
30
HCHE
Heat Exchanger

(c)

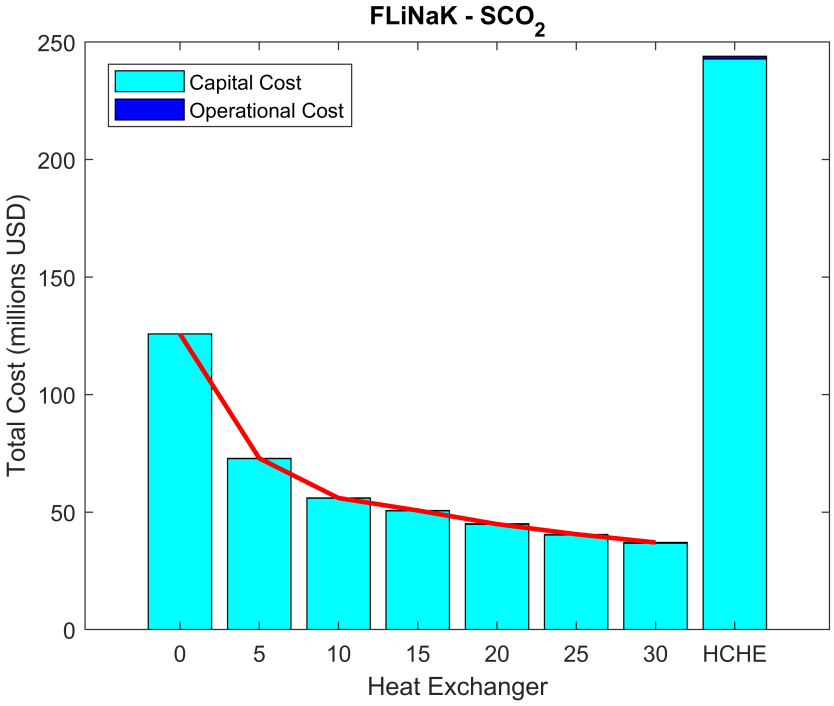
FLiNaK - SCO2
Capital Cost
Operational Cost
Total Cost (millions USD)
0
50
100
150
200
250
0
5
10
15
20
25
30
HCHE
Heat Exchanger

(d)

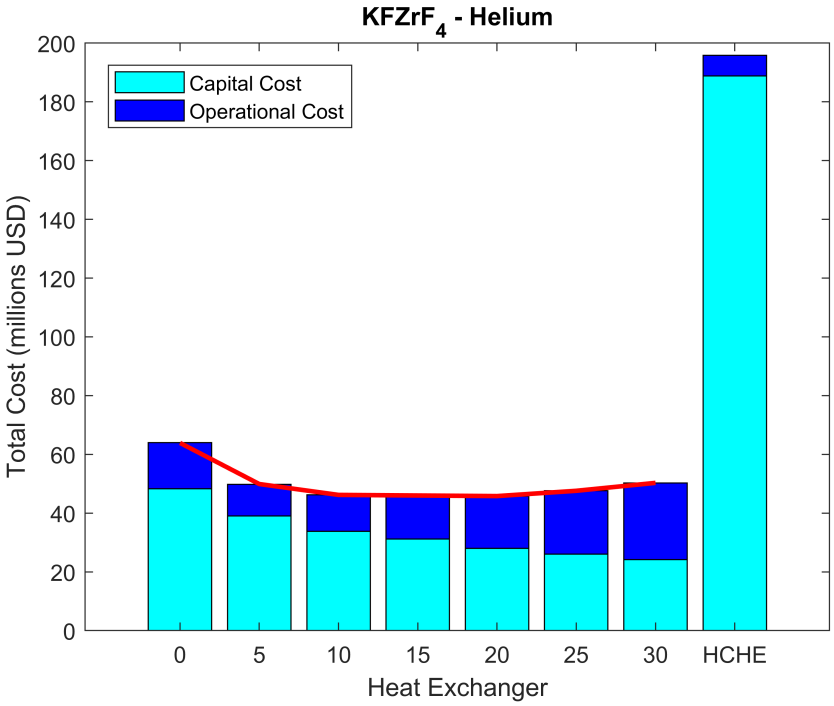

(e)

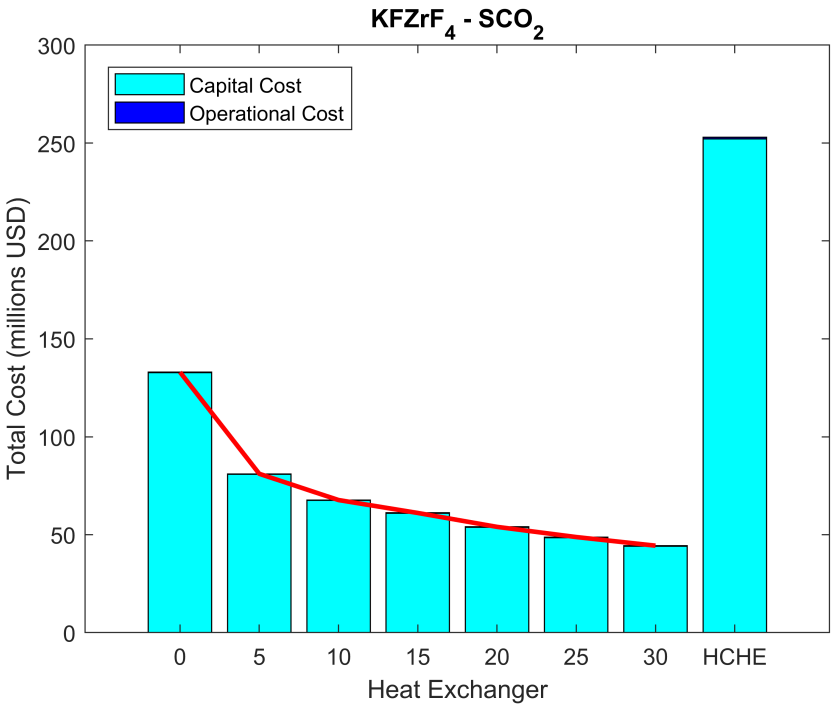

(f)

Figure 5.1: Total cost of HX systems for (a) Helium-Helium, (b) Helium-SCO_2, (c) FLiNaK-Helium, (d) FLiNaK-SCO_2, (e) $KFZrF_4$-Helium, (f) $KFZrF_4$-SCO_2

Table 5.1: Calculated total costs of heat exchangers (in millions USD)

Fluid Sets	PCHE							HCHE
	0°	5°	10°	15°	20°	25°	30°	
He-He	56.8	46.4	45.5	50.2	56.4	65.2	75.9	165.3
He-SCO_2	126.0	74.2	61.8	56.5	51.0	47.5	45.3	214.9
FLiNaK-He	40.3	36.2	33.4	31.9	30.6	30.2	30.1	198.4
FLiNaK-SCO_2	125.8	72.9	56.0	50.7	44.9	40.6	37.1	244.0
$KFZrF_4$-He	63.9	49.9	46.2	46.0	45.8	47.6	50.3	195.7
$KFZrF_4$-SCO_2	133.0	81.1	67.7	61.1	54.0	48.8	44.4	253.0

It is evident from Table 5.1 and the bar plots in 5.1(a) - (f), that the total cost for the HCHEs is significantly larger than both, the straight and zigzag PCHE designs. It can also be seen that for most fluid sets, an increase in the pitch angle results in a decrease in the overall cost of the HX. This can be attributed to the enhanced heat transfer capabilities of zigzag HXs. The only fluid sets where the total cost starts to rise with additional increase in pitch angle are Helium-Helium and $KFZrF_4$-Helium. The two distinct sections of the stacked bar plots provide an insight into the contributions of the capital versus the operating cost for the HX designs. The red line connects the maximum values of the individual bars in the plot and therefore provides information regarding the trend of the HX costs with HX design variance.

For Figures 5.1 (b), (d) and (f), which represent the HXs with SCO_2 as secondary fluid, the capital costs range from 75% of the total cost for Helium-SCO_2 as the fluid set, to almost 98% of the total cost for $KFZrF_4$-SCO_2. This is representative of what has already been established in regards to the HX volumes for fluid sets with SCO_2 as the secondary fluid. The only design in which the operating cost exceeds the capital cost is that of the PCHE zigzag designs for the Helium-Helium fluid set, with pitch angles varying from 10° to 30°. These also happen to be the smallest HX designs acquired during this study. Nevertheless, it can be seen from Table 5.1 that the lowest total costs for the PCHE designs occur for the fluid set of FLiNaK-Helium. This suggest that although the capital costs for HXs designs with Helium-Helium are low due to the Helium's high

thermal conductivity and heat capacity when compared to molten salts, the operational costs which are based off the pumping power are high due to the Helium's low density, thus contributing to larger total costs. Figure 5.2 plots the data provided in Table 5.1 and provides insight into the effect of changes in pitch angles on the total costs of the PCHEs.

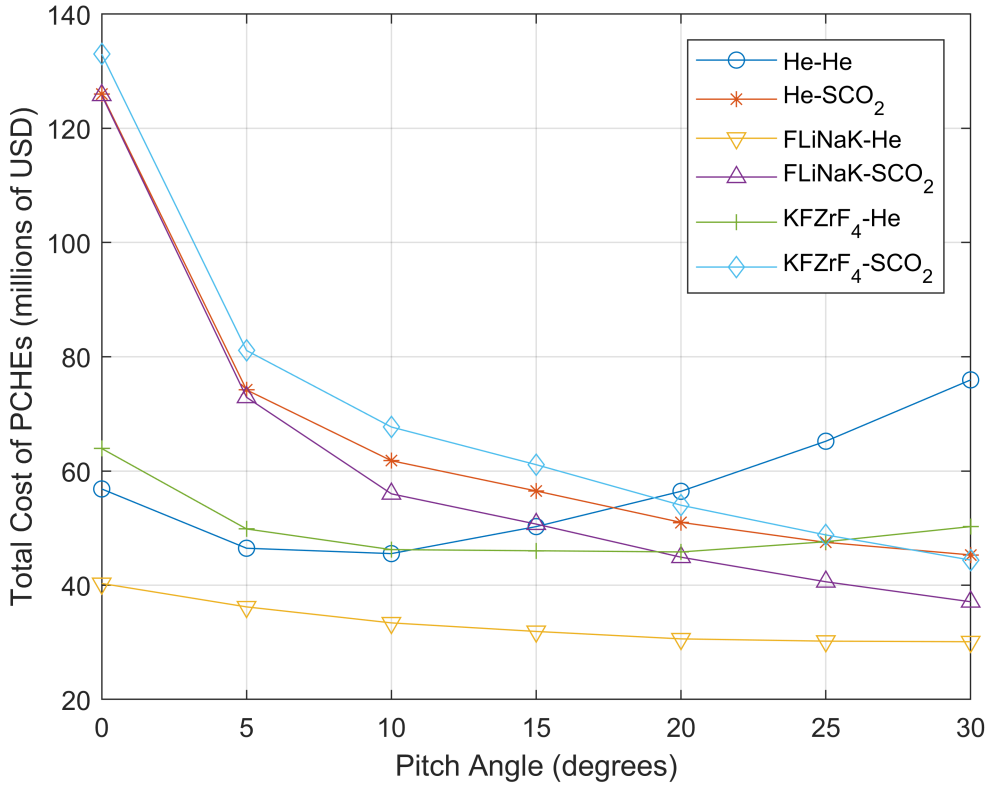

Figure 5.2: Effect of pitch angle on total costs of PCHEs

The drop in total costs, when switching from straight PCHEs to the zigzag designs, is another representation of the significant effects of increments in pitch angles on the HX volumes. For HXs with SCO_2 as their secondary fluid, the costs decrease by over 40% when moving from straight to zigzag PCHEs with a pitch angle of 5°. In HXs with Helium as their secondary fluid, the costs decrease by about 20% for the same change in HX design. It can be seen from Figure 5.2 that the costs of PCHEs for Helium-Helium and $KFZrF_4$-Helium reach a minimum for pitch angles of 10° and 20° respectively, and then

start to increase. This indicates that for the fluids sets in concern, the HX operational costs start becoming the major contributing factor to the total costs. Thus, although an increases in pitch angles would lead to HXs with smaller volumes and therefore with lower capital costs, the pressure drops that need to be overcome increase significantly, therefore increasing the operational costs. This shows that the total costs in the case of these fluid sets is mainly driven by the operational costs. As for fluid sets other than Helium-Helium and $KFZrF_4$-Helium, their total costs are mainly driven by the capital costs, and therefore have a declining trend with further increments in pitch angles. The total HX costs are lowest for FLiNaK-Helium as it has some of the best FOM values, along with smaller HX volumes. This is supported by plots in Figures 4.1, 4.3, and 4.4.

CHAPTER 6

Conclusions and Future Work

This chapter outlines the milestones that were achieved during this study by using the conclusions that were drawn from the results of the HX sizing and cost analyses, and provides some directions for future work. Section 6.1 recaps the most important points from Chapter 1, 2, and 3, whereas Section 6.2 summarizes the main results from the HX sizing and performance analyses. Section 6.3 condenses the cost analysis that was performed in Chapter 5, and then leads into the recommendations for future work.

6.1 Summary

Sizing and cost analyses of compact and conventional HXs was carried out in this study to provide quantifiable metrics, in order to compare the thermal performance and the economic benefits of one design over the other. While extensive studies have been conducted for the HX designs studied herein, little to no information is available on how they fare when compared to one another. For this study, straight and zigzag channeled PCHEs were compared to a conventional HCHE. Using various fluid sets at different operating conditions, geometry specific thermal hydraulic correlations, and reasonable boundary conditions, mathematical models were derived to acquire merit categories based on which the HXs could be compared. In conclusion, it was found that the PCHEs performed more efficiently in terms of sizing as well as thermal performances when compared to HCHEs.

6.2 Modeling Analyses

- PCHEs are superior when compared to HCHEs in terms of sizing and thermal hydraulic performance.

- HXs with Helium as the secondary fluid were smaller in size when compared to those with SCO_2. The total costs however were dependent on the pitch angles chosen for the design (see Figure 5.2).
- The FOM_1 values for PCHEs and HCHEs vary by a factor of about 2 - 4 for HXs with Helium as the secondary fluid. In the case of HXs with SCO_2 as the secondary fluid, the same variance is by a factor of about 5 - 8. For a combination of specific fluid set, operating conditions and design constraints, there exist optimum pitch angles for PCHEs that would result in better thermal performance.
- In terms of the FOM_2, increments in pitch angles lead to increased pressure drops per unit length. These values are however significantly lower for HCHE designs due to their relatively long tube lengths.
- The HX compactness increases by 15% when moving from straight PCHEs to zigzag designs with a pitch angle of 30°. In comparison, the HCHE compactness is smaller by a factor of 10.
- From Figure 4.4, it can also be seen that for HXs with Helium as the secondary fluid, the pressure drops per unit length are higher. This can be attributed to the fact that HXs with SCO_2 as the secondary fluid are larger in volume, thus having more channels which lead to lower fluid mass flow rates through each channel. Low mass flow rates result in lower fluid velocities, and therefore lower pressure drops.
- The sizing plots provide evidence to the fact that the nature of the fluids used in the HXs and their operating conditions drive its required physical dimensions and the thermal performance significantly.

6.3 Cost Analyses

- As fabrication costs of neither the HX designs were taken into consideration, it is difficult to say for certain which HX systems would cost less. However, if it was

assumed that the fabrication costs for each of the PCHE designs was equal to their material cost, or if assumed that the fabrication costs for PCHEs and HCHEs were the same, PCHEs would still end up being cheaper than just the material costs of their HCHE counterparts for the same fluid sets. Thus it can be inferred that PCHEs would end up being cheaper when compared to HCHEs for all the fluid sets considered for this study.

- For Helium-Helium and $KFZrF_4$-Helium based PCHEs, there exist optimum pitch angles for which the total cost is the lowest. For further increments in pitch angles, the total costs increases as the operational costs increase. For all other fluid sets, an increase in pitch angle, decreases the total HX cost.

This study was performed as a first step towards acquiring metrics that would allow for quantitative comparison between compact and conventional HXs. It provided an overview of how the HX designs fare when compared to one another in terms of size and thermal performance. Further studies would include a detailed cost analysis which would take into account the additional components required to connect the PCHE modules in parallel, as well as thermal hydraulic analysis to take into account the additional pressure drops from those components. A detailed cost analysis would also included fabrication and installation costs for the various HX designs, the costs of fluids that are used in the HXs, as well as the pumps and compressor requirements for these various fluids. It is possible that an expensive fluid may perform better but cause the capital costs to skyrocket, and this fact would lead to another factor for HX design optimization.

Structural analysis of HXs would also be considered before making a final decision for the design selection. Thermal and mechanical stresses would affect different HX designs in different ways, and thus need to be studied in detail. Although compact HXs have better thermal performances when compared to HCHEs, there is very little knowledge on the maintenance and inspection costs that would incur for an array of PCHE modules, which

would replace the conventional HXs. Inclusion of more HX designs such as the spiral HX, fluted-tube HX, and shell and tube HX would broaden the scope of analysis and provide more concrete data in terms of thermal performances of compact and conventional HXs. A parametric study could also be performed using tools such as Aspen HYSYS, which would allow for steady state as well as dynamic studies of HXs coupled with power cycles in order to see the effect of changes in HX geometry on the thermal efficiency of the power overall cycle.

This study has provided a simplistic model for comparison of compact and conventional HXs, and will prove to be a stepping stone in order to further the research required to support the development and deployment of compact HXs.

Bibliography

[1] "U.S. Energy Information Administration," https://www.eia.gov/outlooks/ieo/, accessed: 2018-04-28.

[2] "Nuclear Power in the World Today," http://www.world-nuclear.org/information-library/current-and-future-generation/nuclear-power-in-the-world-today.aspx, accessed: 2018-01-19.

[3] "A Technology Roadmap for Generation IV Nuclear Energy Systems," https://www.gen-4.org/gif/jcms/c_40473/a-technology-roadmap-for-generation-iv-nuclear-energy-systems, accessed: 2017-08-09.

[4] T. Abram and S. Ion, "Generation-IV nuclear power: A review of the state of the science," *Energy Policy*, vol. 36, no. 12, pp. 4323–4330, 2008.

[5] C. M. Stoots, J. E. O'Brien, K. G. Condie, and J. J. Hartvigsen, "High-temperature electrolysis for large-scale hydrogen production from nuclear energy–experimental investigations," *International Journal of Hydrogen Energy*, vol. 35, no. 10, pp. 4861–4870, 2010.

[6] P. Sabharwall, E. S. Kim, M. McKellar, N. Anderson, and M. Patterson, "Process heat exchanger options for the advanced high temperature reactor," *INL/EXTY11Y21584, Idaho National Laboratory*, 2011.

[7] Q. Li, G. Flamant, X. Yuan, P. Neveu, and L. Luo, "Compact heat exchangers: A review and future applications for a new generation of high temperature solar receivers," *Renewable and Sustainable Energy Reviews*, vol. 15, no. 9, pp. 4855–4875, 2011.

[8] "Heatric," https://www.heatric.com/diffusion_bonded_heat_exchangers.html, accessed: 2017-08-01.

[9] K. Nikitin, Y. Kato, and L. Ngo, "Printed circuit heat exchanger thermal–hydraulic performance in supercritical CO_2 experimental loop," *International Journal of Refrigeration*, vol. 29, no. 5, pp. 807–814, 2006.

[10] T. L. Ngo, Y. Kato, K. Nikitin, and N. Tsuzuki, "New printed circuit heat exchanger with s-shaped fins for hot water supplier," *Experimental Thermal and Fluid Science*, vol. 30, no. 8, pp. 811–819, 2006.

[11] S. Mylavarapu, X. Sun, J. Figley, N. Needler, and R. Christensen, "Investigation of high-temperature printed circuit heat exchangers for very high temperature reactors," *Journal of Engineering for Gas Turbines and Power*, vol. 131, no. 6, p. 062905, 2009.

[12] I. H. Kim and H. C. No, "Physical model development and optimal design of PCHE for intermediate heat exchangers in HTGRs," *Nuclear Engineering and Design*, vol. 243, pp. 243–250, 2012.

[13] S. Baek, J.-H. Kim, S. Jeong, and J. Jung, "Development of highly effective cryogenic printed circuit heat exchanger (PCHE) with low axial conduction," *Cryogenics*, vol. 52, no. 7-9, pp. 366–374, 2012.

[14] "International Energy Outlook 2017," https://www.eia.gov/tools/faqs/faq.php?id=19&t=3, accessed: 2017-10-25.

[15] C. Fuller, "Fort Saint Vrain Operational Experience," *Design Requirements, Operation and Maintenance of Gas-Cooled Reactors*, 1989.

[16] D. Aquaro and M. Pieve, "High temperature heat exchangers for power plants: Performance of advanced metallic recuperators," *Applied Thermal Engineering*, vol. 27, no. 2-3, pp. 389–400, 2007.

[17] D. LeBlanc and C. Rodenburg, "Integral molten salt reactor," in *Molten Salt Reactors and Thorium Energy*. Elsevier, 2017, pp. 541–556.

[18] C. W. Shin and H. C. No, "Experimental study for pressure drop and flow instability of two-phase flow in the pche-type steam generator for smrs," *Nuclear Engineering and Design*, vol. 318, pp. 109–118, 2017.

[19] R. K. Shah and D. P. Sekulić, "Classification of heat exchangers," *Fundamentals of Heat Exchanger Design*, pp. 1–77, 2007.

[20] J. Gunnarsson, I. Sinclair, and F. J. Alanis, "Compact Heat Exchangers: Improving Heat Recovery," *Chemical Engineering*, vol. 116, no. 2, p. 44, 2009.

[21] S. K. Mylavarapu, "Development of Compact Heat Exchangers for Very High-Temperature Gas-Cooled Reactors," Master's thesis, The Ohio State University, 2008.

[22] "Sentry Equipment," https://sentry-equip.com/sentry-spiral-tube-heat-exchanger.html, accessed: 2017-07-04.

[23] "Coil-wound heat exchanger," https://www.linde-engineering.com/en/plant_components/coil_wound_heat_exchangers/, accessed: 2018-07-15.

[24] M. Chen, "Design, Fabrication, Testing, and Modeling of a High-temperature Printed Circuit Heat Exchanger," Master's thesis, The Ohio State University, 2015.

[25] "High Temperature Metals," http://www.hightempmetals.com/techdata/hitempInconel617data.php, accessed: 2017-08-01.

[26] N. Anderson and P. Sabharwall, "Molten salt mixture properties (KF-ZrF_4 and KCl-$MgCl_2$) for use in RELAP5-3D for high-temperature reactor application," *Nuclear technology*, vol. 178, no. 3, pp. 335–340, 2012.

[27] K. Gezelius, "Design of compact intermediate heat exchangers for gas cooled fast reactors," Master's thesis, Massachusetts Institute of Technology, 2004.

[28] J. E. Hesselgreaves, R. Law, and D. Reay, *Compact heat exchangers: selection, design and operation*. Butterworth-Heinemann, 2016.

[29] G. F. Hewitt, *Heat exchanger design handbook, 1998*. New York: Begell House, 1998.

Appendix: Heat Exchanger Sizing Codes

The codes provided here describe the sizing and thermal hydraulic calculations that were performed for Helium-Helium fluid set. The calculations for other fluid sets only required modifications in terms of the thermophysical properties that were to be used.

```
%************************************************************************
%************************************************************************
clc
clear all

%==========PRINTED CIRCUIT HEAT EXCHANGER - STRAIGHT==========
%Fluid Set: Helium - Helium

%Heat Exchanger Performance Parameters
Q=400000;  %Duty in kW

HX_eps=1;   %HX Effectiveness initializer
Th_o_C=525; %Hot fluid outlet temperature assumption in C

while(HX_eps>=0.92) %Conditional loop to calculate hot outlet temperature
%---Temperatures---
%---Cold Fluid---
Tc_i_C=520.0; %Cold fluid inlet temperature in C
Tc_o_C=776.0; %Cold fluid outlet temperature in C
Tc_avg_C=(Tc_i_C+Tc_o_C)/2; %Average cold fluid temperature in C

%Hot Fluid
Th_i_C=800.0;                %Hot fluid inlet temperature in C
Th_avg_C=(Th_i_C+Th_o_C)/2;   %Average hot fluid temperature in C

Pressure=7000;  %Operating pressure at fluid inlet in kPa
cp_he=5193;     %Heat Capacity of Helium in J/kg-K

%---Mass flow rates---
m_hot=Q*1000/(cp_he*abs(Th_i_C-Th_o_C));   %Hot fluid mass flow rate in kg/
   s
m_cold=Q*1000/(cp_he*abs(Tc_i_C-Tc_o_C));  %Cold fluid mass flow rate in kg
   /s

%---Heat Rates---
C_hot=m_hot*cp_he;          %Heat capacity rate of hold fluid in W/K
C_cold=m_cold*cp_he;        %Heat capacity rate of cold fluid in W/K
C_min=min(C_hot,C_cold);    %Minimum heat capacity rate in W/K

%---Effectiveness---
Q_max=C_min*(Th_i_C-Tc_i_C)/1000;   %Maximum heat transfer rate in W
HX_eps=Q/Q_max;      %HX effectiveness
Th_o_C=Th_o_C+0.1;   %Hot fluid outlet temperature increment in C
```

```
end

%---LMTD---
DT1=Th_i_C-Tc_o_C;    %Temperature difference at end 1
DT2=Th_o_C-Tc_i_C;    %Temperature difference at end 2
LMTD=(DT2-DT1)/(log(DT2/DT1)); %Log mean temperature difference

%---UA--- Overall heat transfer coeff*Area of heat transfer
UA=Q*1000/LMTD ; %UA in W/C

%---Channel Dimensions---
d=0.002;    %Channel diameter in m
cp=0.0025;  %Channel pitch in m
tp=0.00163; %Plate thickness in m
t_eff=tp-pi()/8*d;  %Effective wall thickness in m
Dh=pi()*d/(pi()+2); %Hydraulic diameter of semicircular channel in m
A_f_ch=pi()*d^2/8;  %Flow area per channel in m^2

%Minimum number of channels required for laminar flow
Rey_max=2200;                                          %Laminar reynolds
   number
N_ch_he_cold=m_cold*Dh/(Rey_max*mu_he(Tc_avg_C)*A_f_ch); %Num. channels
   based on cold fluid flow
N_ch_he_hot=m_hot*Dh/(Rey_max*mu_he(Th_avg_C)*A_f_ch);   %Num. channels
   based on hot fluid flow
N_ch_max=max(N_ch_he_cold, N_ch_he_hot);                %Max num of
   channels
A_f_tot=A_f_ch*N_ch_max;                                %Total flow area
   in m^2

N=N_ch_max;                 %Number of channels as initial guess
i=0;                        %Initialize counter
L_HX=1.5;                   %Initialize length of HX in m
del_P_max=0.01*Pressure;    %Intialize pressure drop in HX in kPa

while(del_P_max>=0.01*Pressure)||(L_HX>=1.5)    %Conditional Loop

    %---Heat transfer areas---
    k_ss=23;                        %Thermal conductivity of Alloy 617 in W
       /m-K
    w_ave=(tp*d-pi()*d^2/8)/t_eff;  %Average width in m
    A_cond=w_ave*N;                 %Area of conduction per length in m
    A_ht=(pi()*d/2+d)*N;            %Area of heat transfer per length in m
    A_f_tot=A_f_ch*N;               %Total flow area in m^2

    %---Flow conditions---
    vel_hot=m_hot/(rho_he(Th_avg_C)*A_f_tot);       %Velocity of hot fluid
       in m/s
    vel_cold=m_cold/(rho_he(Tc_avg_C)*A_f_tot);     %Velocity of hot fluid
       in m/s
```

```
    Rey_hot=m_hot*Dh/(A_f_tot*mu_he(Th_avg_C));     %Reynolds number for
       hot fluid
    Rey_cold=m_cold*Dh/(A_f_tot*mu_he(Tc_avg_C));   %Reynolds number for
       cold fluid

    Pr_hot=cp_he*mu_he(Th_avg_C)/k_he(Th_avg_C);    %Prandtl number hot
       fluid
    Pr_cold=cp_he*mu_he(Tc_avg_C)/k_he(Tc_avg_C);   %Prandtl number cold
       fluid

    %---Friction factors---
    f_hot=15.78/Rey_hot;    %Hot fluid Fanning friction factor
    f_cold=15.78/Rey_cold;  %Cold fluid Fanning friction factor

    %---Nusselt Numbers---
    Nu_hot=4.089;   %Hot fluid Nusselt number
    Nu_cold=4.089;  %Cold fluid Nusselt number

    %---Convective Heat Transfer Coefficients---
    h_hot=Nu_hot.*k_he(Th_avg_C)/Dh;    %Hot fluid convective heat transfer
        coefficient in W/m^2-C
    h_cold=Nu_cold.*k_he(Tc_avg_C)/Dh;  %Cold fluid convective heat
       transfer coefficient in W/m^2-C

    %---Overall Heat Transfer Coefficient---
    U=(1/h_hot+(t_eff/k_ss)*(A_ht/A_cond)+1/h_cold)^(-1.0);  %Overall heat
       transfer coefficient in W/m2-C

    %---Area of Heat Transfer---
    A_HT=UA/U;  %Heat transfer area on HX in m^2

    %---Length of Heat Exchanger---
    L_HX=A_HT/(N*(pi()*d/2+d)); %Length of HX in m

    %---Pressure Drop---
    del_P_h=(f_hot*(4*L_HX/Dh)*(rho_he(Th_avg_C)*vel_hot^2.0/2))/10^3;
            %Pressure drop in hot fluid in kPa
    del_P_c=(f_cold*(4*L_HX/Dh)*(rho_he(Tc_avg_C)*vel_cold^2.0/2))/10^3;
          %Pressure drop in cold fluid in kPa
    del_P_max=max(del_P_h, del_P_c);    %Maximum pressure drop in kPa

    i=i+1;  %Counter addition
    N=N+1;  %Number of channels addition
end

%---Volume Calculations---
num_channels=240;                 %Number of channels per plate
num_plates=floor(N/num_channels); %Number of plate (Just hot plates)
width_HX=cp*num_channels;         %Width of PCHE plate in m
height_HX=2*tp*num_plates;        %Heigth of PCHE in m
Volume=width_HX*height_HX.*L_HX;  %Volume of PCHE in m^3
Compactness=A_HT/Volume;          %Compactness in m^2/m^3
```

```
Num_modules=Volume./(3.*L_HX.*width_HX); %Number of HX modules


%---Figures of Merit---
FOM1=U/del_P_max;       %Overall heat transfer coefficient per pressure
    drop
FOM2=del_P_max/L_HX;    %Overall pressure drop per length of HX

%---Pumping Work---
W_cold=del_P_c*m_cold/rho_he(Tc_avg_C); %Cold side pumping power in kW
W_hot=del_P_h*m_hot/rho_he(Th_avg_C);   %Hot side pumping power in kW
W_max=max(W_cold,W_hot);                %Maximum pumping power in kW

%==================COST ANALYSIS==============================
rho_mat=8360;   %Density of Alloy 617 in kg/m^3
Cost_mat=120;   %Cost of Alloy 617 in $/kg
Cost_elec=0.12; %Cost of electricity in $/kWh
Num_years=10;   %Number of operational years

%---Total HX Material Calculations---
V_ch=pi()*d^2/8*L_HX;   %Volume of a single channel in m^3
V_void=V_ch*N;          %Total void volume (volume occupied by fluid) in m
    ^3
V_mat=Volume-V_void;    %Material volume of HX in m^3
M_mat=V_mat*rho_mat;    %Mass of HX material in kg

%---Pricing---
CapCost_HX=M_mat*Cost_mat;                  %Capital cost of HX in USD
OpCost_HX=W_max*Cost_elec*Num_years*24*365; %Operating cost of HX in USD
TotalCost_HX=CapCost_HX+OpCost_HX;          %Total cost of HX in USD

%=====END OF CODE FOR PCHE STRAIGHT=====%
%************************************************************************
%************************************************************************
```

```
%*************************************************************************
%*************************************************************************
clc
clear all

%==========PRINTED CIRCUIT HEAT EXCHANGER - ZIGZAG==========
%Fluid Set: Helium - Helium

%Heat Exchanger Performance Parameters
Q=400000; %Duty in kW

HX_eps=1;   %HX Effectiveness initializer
Th_o_C=525; %Hot fluid outlet temperature assumption in C

while(HX_eps>=0.92) %Conditional loop to calculate hot outlet temperature
%---Temperatures---
%---Cold Fluid---
Tc_i_C=520.0; %Cold fluid inlet temperature in C
Tc_o_C=776.0; %Cold fluid outlet temperature in C
Tc_avg_C=(Tc_i_C+Tc_o_C)/2; %Average cold fluid temperature in C

%Hot Fluid
Th_i_C=800.0; %Hot fluid inlet temperature in C
Th_avg_C=(Th_i_C+Th_o_C)/2;  %Average hot fluid temperature in C

Pressure=7000; %Operating pressure in kPa
cp_he=5193;    %Heat Capacity of Helium J/kg-K

%---Mass flow rates---
m_hot=Q*1000/(cp_he*abs(Th_i_C-Th_o_C));   %mass flow rate in kg/s
m_cold=Q*1000/(cp_he*abs(Tc_i_C-Tc_o_C));  %mass flow rate in kg/s

%---Heat Rates---
C_hot=m_hot*cp_he;          %Heat capacity rate of hold fluid in W/K
C_cold=m_cold*cp_he;        %Heat capacity rate of cold fluid in W/K
C_min=min(C_hot,C_cold);    %Minimum heat capacity rate in W/K

%---Effectiveness---
Q_max=C_min*(Th_i_C-Tc_i_C)/1000;   %Maximum heat transfer rate in W
HX_eps=Q/Q_max;      %HX effectiveness
Th_o_C=Th_o_C+0.1;   %Hot fluid outlet temperature increment in C
end

%---LMTD---
DT1=Th_i_C-Tc_o_C;    %Temperature difference at end 1 in K
DT2=Th_o_C-Tc_i_C;    %Temperature difference at end 2 in K
LMTD=(DT2-DT1)/(log(DT2/DT1)); %Log mean temperature difference in K

%---UA---Overall heat transfer coeff*Area of heat transfer
UA=Q*1000/LMTD ; %UA in W/K

%---Pitch Angle---
```

```
phi_d=5:5:30;            %pitch angle in degrees
phi_r=phi_d*pi()./180;   %pitch angle in radians

%---Channel Dimensions---
cd=0.002;                %Channel diameter in m
p=0.0246;                %Single pitch length in m
cp=0.0025;               %Channel pitch in m
tp=0.00163;              %Plate thickness in m
t_eff=tp-pi()/8*cd;      %Effective wall thickness in m
Dh=pi()*cd/(pi()+2);     %Hydraulic diameter of semicircular channel in m
A_f_ch=pi()*cd^2/8;      %Flow area per channel in m^2

%---Minimum number of channels required for laminar flow---
Rey_max=2200; %Laminar reynolds number
N_ch_he_cold=m_cold*Dh/(Rey_max*mu_he(Tc_avg_C)*A_f_ch); %Num. channels
   based on cold fluid flow
N_ch_he_hot=m_hot*Dh/(Rey_max*mu_he(Th_avg_C)*A_f_ch);  %Num. channels
   based on hot fluid flow
N_ch_max=max(N_ch_he_cold, N_ch_he_hot);    %Max num of channels
A_f_tot=A_f_ch*N_ch_max; %Total flow area

%---Kim's correlation constants---
a=[0.0034,0.02342,0.06677,0.12748,0.17458,0.25418];
b=[1.0502,0.8863,0.81258,0.78473,0.79345,0.7867];
c=[0.00071,0.00314,0.0083,0.01703,0.02182,0.0299];
d=[1.10341,0.96567,0.86054,0.79007,0.77285,0.7403];

%**************************************************************************
%==========================================================================
%Constraints herein are as follows
%   1)Allowable pressure drop is 1% of maximum operating pressure drop
%   2)Length of HX channel needs to be a maximum of 1.5m
%   3)Flow needs to be laminar (Re<=2200)
%==========================================================================
%**************************************************************************


for j=1:1:length(phi_d)
    %Initial guesses for while loop
    del_P_max(j)=0.01*Pressure+5; %Pressure drop initialize
    L_calc(j)=1.5;           %Channel length initialize
    Rey_max_calc=2200;       %Maximum Reynolds number
    i=1;                     %Loop iteration counter
    N=N_ch_max;              %Number of channels required for laminar flow

    while(del_P_max(j)>=0.01*Pressure) || (L_calc(j)>=1.5) %Conditional
       loop for HX sizing
        %---Heat transfer and flow parameters---
        k_ss=23;                          %Thermal conductivity of Alloy
           617 in W/m-K
        w_ave=(tp*cd-pi()*cd^2/8)/t_eff;  %Average width in m
        A_cond=w_ave*N;                   %Area of conduction per length in
```

```
    m
A_f_tot=A_f_ch*N;                  %Total flow area in m^2
A_ht=(pi()*cd/2+cd)*N;             %Heat transfer area per length in
    m

%---Flow conditions---
vel_hot=m_hot./(rho_he(Th_avg_C).*A_f_tot);   %Velocity of hot
   fluid in m/s
vel_cold=m_cold./(rho_he(Tc_avg_C).*A_f_tot); %Velocity of cold
   fluid in m/s

Rey_hot=m_hot.*Dh./(A_f_tot.*mu_he(Th_avg_C));    %Reynolds number
   for hot fluid
Rey_cold=m_cold.*Dh./(A_f_tot.*mu_he(Tc_avg_C));  %Reynolds number
   for cold fluid
Rey_max_calc=max(Rey_hot,Rey_cold);               %Maximum Reynolds
    number
Max_Reynolds(j)=Rey_max_calc;

Pr_hot=cp_he*mu_he(Th_avg_C)/k_he(Th_avg_C);    %Prandtl number hot
    fluid
Pr_cold=cp_he*mu_he(Tc_avg_C)/k_he(Tc_avg_C);   %Prandtl number
   cold fluid

%---Friction factors---
%---Kim's correlations where Dh=1.22mm and Pitch=24.6mm---
f_hot(j)= (15.78+a(j).*Rey_hot.^b(j))./Rey_hot;    %Fanning
   friction hot fluid
f_cold(j)= (15.78+a(j).*Rey_cold.^b(j))./Rey_cold; %Fanning
   friction cold fluid

%---Nusselt Number Correlations---
%---Kim's correlations where Dh=1.22mm and Pitch=24.6mm---
Nu_hot(j)=4.089+c(j).*Rey_hot.^d(j);   %Nusselt number hot fluid
Nu_cold(j)=4.089+c(j).*Rey_cold.^d(j); %Nusselt number cold fluid

%---Convective Heat Transfer Coefficients---
h_hot(j)=Nu_hot(j).*k_he(Th_avg_C)./Dh;    %hot fluid convective
   heat transfer coefficient in W/m2-K
h_cold(j)=Nu_cold(j).*k_he(Tc_avg_C)./Dh;  %cold fluid convective
   heat transfer coefficient in W/m2-K

%---Overall Heat Transfer Coefficient---
U(j)=(1./h_hot(j)+(t_eff/k_ss).*(A_ht./A_cond)+1./h_cold(j))
   .^(-1.0);   %Overall heat transfer coefficient in W/m2-K

%---Area of Heat Transfer---
A_HT(j)=UA./U(j);  %Heat exchanger heat transfer area in m^2

%---Length of HX channels---
L_calc(j)=A_HT(j)./A_ht;  %Heat exchanger channel length in m
```

```
        %---Pressure Drop---
        del_P_h=(f_hot.*(4.*L_calc./Dh).*(rho_he(Th_avg_C).*vel_hot
            .^2.0./2))./10^3; %Pressure drop in hot fluid in kPa
        del_P_c=(f_cold.*(4.*L_calc./Dh).*(rho_he(Tc_avg_C).*vel_cold
            .^2.0./2))./10^3;     %Pressure drop in cold fluid in kPa
        del_P_max=max(del_P_c,del_P_h); %Max pressure drop in kPa

        i=i+1;  %Counter for loop
        N=N+1;  %Increment in number of channels
    end
    max_dp(j)=del_P_max(j); %Max allowed pressure drop for each pitch angle
    Ns(j)=N;   %Max number of channels for each pitch angle
end

%---Volume Calculations---
num_channels=235;                   %number of channels per plate
num_plates=floor(Ns./num_channels); %number of plate (just hot | will have
    to double for total of hot and cold)
width_HX=(p/2)*tan(phi_r)+num_channels*cp; %Width of HX plate in m
height_HX=2*tp*num_plates;          %Heigth of PCHE in m
L_HX=L_calc.*cos(phi_r);            %Length of PCHE in m
Volume=width_HX.*height_HX.*L_HX;   %Volume of PCHE in m^3
Compactness=A_HT./Volume;           %Compactness in m^2/m^3
Num_modules=Volume./(3.*L_HX.*width_HX); %Number of HX modules

%---Figures of Merit---
FOM1=U./del_P_max;       %Overall heat transfer coefficient per pressure
    drop
FOM2=del_P_max./L_calc;  %Overall pressure drop per length of HX


%----Pumping Work---
W_cold=del_P_c.*m_cold./rho_he(Tc_avg_C); %Cold side pumping power in kW
W_hot=del_P_h.*m_hot./rho_he(Th_avg_C);   %Hot side pumping power in kW
W_max=max(W_cold,W_hot);                  %Maximum pumping power in kW

%==================COST ANALYSIS==============================
rho_mat=8360;   %Density of Alloy 617 in kg/m^3
Cost_mat=120;   %Cost of Alloy 617 in $/kg
Cost_elec=0.12; %Cost of electricity in $/kWh
Num_years=10;   %Number of operational years


%---Total HX Material Calculations---
V_ch=pi()*cd^2./8.*L_calc;   %Volume of a single channel in m^3
V_void=V_ch.*Ns;             %Total void volume (volume occupied by fluid)
    in m^3
V_mat=Volume-V_void;         %Material volume of HX in m^3
M_mat=V_mat.*rho_mat;        %Mass of HX material in kg

%---Pricing---
CapCost_HX=M_mat.*Cost_mat;                 %Capital cost of HX in USD
```

```
OpCost_HX=W_max.*Cost_elec*Num_years*24*365; %Operating cost of HX in USD
TotalCost_HX=CapCost_HX+OpCost_HX;           %Total cost of HX in USD

%=====END OF CODE FOR PCHE ZIGZAG=====%
%**************************************************************************
%**************************************************************************
```

```
clc
clear all

%==========HELICAL COIL HEAT EXCHANGER==========
%Fluid Set: Helium - Helium

%Heat Exchanger Performance Parameters
Q=400000; %Duty (kW)

HX_eps=1;   %HX Effectiveness initializer
Th_o_C=525; %Hot fluid outlet temperature assumption in C

while(HX_eps>=0.92) %Conditional loop to calculate hot outlet temperature
%---Temperatures---
%---Cold Fluid---
Tc_i_C=520.0; %Cold fluid inlet temperature in C
Tc_o_C=776.0; %Cold fluid outlet temperature in C
Tc_avg_C=(Tc_i_C+Tc_o_C)/2; %Average cold fluid temperature in C

%Hot Fluid
Th_i_C=800.0; %Hot fluid inlet temperature in C
Th_avg_C=(Th_i_C+Th_o_C)/2;  %Average hot fluid temperature in C

Pressure=7000;  %Operating pressure at fluid inlet in kPa
cp_he=5193;     %Heat Capacity of Helium in J/kg-K

%---Mass flow rates---
m_hot=Q*1000/(cp_he*abs(Th_i_C-Th_o_C));   %mass flow rate in kg/s
m_cold=Q*1000/(cp_he*abs(Tc_i_C-Tc_o_C));  %mass flow rate in kg/s

%---Heat Rates---
C_hot=m_hot*cp_he;          %Heat capacity rate of hold fluid in W/K
C_cold=m_cold*cp_he;        %Heat capacity rate of cold fluid in W/K
C_min=min(C_hot,C_cold);    %Minimum heat capacity rate in W/K

%---Effectiveness---
Q_max=C_min*(Th_i_C-Tc_i_C)/1000;   %Maximum heat transfer rate in W
HX_eps=Q/Q_max;      %HX effectiveness
Th_o_C=Th_o_C+0.1;   %Hot fluid outlet temperature increment in C
end

%---LMTD---
DT1=Th_i_C-Tc_o_C;    %Temperature difference at end 1
DT2=Th_o_C-Tc_i_C;    %Temperature difference at end 2
LMTD=(DT2-DT1)/(log(DT2/DT1)); %Log mean temperature difference

%---UA--- Overall heat transfer coeff*Area of heat transfer
UA=Q*1000/LMTD ; %UA in W/C

%---Pipe dimensions---
IT_id_in=0.402;     IT_id_m=IT_id_in*0.0254;   %Inner tube inner diameter
IT_od_in=0.5;       IT_od_m=IT_od_in*0.0254;   %Inner tube outer diameter
```

```
OT_id_in=0.834;     OT_id_m=OT_id_in*0.0254;   %Outer tube inner diameter
OT_od_in=1;         OT_od_m=OT_od_in*0.0254;   %Outer tube outer diameter

%---Pipe material property---
k_p=23;  %Thermal conductivity of Alloy 617 in W/m-K

%---Hydraulic diameter of Annulus---
Dh=OT_id_m-IT_od_m;     %Annular Hydraulic diameter in m

%---Coil Dimensions---
width_in=98.4; width_m=width_in*0.0254;  %coil width in inches and meters
    (2.5m)
r_curv=width_m/2-OT_od_m/2;     %radius of curvature in m
d_curv=r_curv*2;                %diameter of curvature in m

%---Number of tubes---
N=5000; %Initial guess for number of HX tubes

i=0;    %Loop counter initialize
del_P_max=0.01*Pressure;   %Maximum allowable pressure drop in kPa
while(del_P_max>=0.01*Pressure) %Conditional loop for HX sizing

%---Flow Area---
A_f_p=N*pi*IT_id_m^2/4.0;               %Hot fluid flow area in m^2
A_f_s=N*pi*(OT_id_m^2-IT_od_m^2)/4.0;    %Cold fluid flow area (annulus) in
     m^2

%---Fluid Velocity---
vel_h=m_hot/(rho_he(Th_avg_C)*A_f_p);     %Hot fluid velocity in m/s
vel_c=m_cold/(rho_he(Tc_avg_C)*A_f_s);    %Cold fluid velocity in m/s

%---Reynolds Number---
Rey_h=rho_he(Th_avg_C)*vel_h*IT_id_m/mu_he(Th_avg_C);  %Hot fluid reynolds
    number
Rey_c=rho_he(Tc_avg_C)*vel_c*Dh/mu_he(Tc_avg_C);       %Cold fluid reynolds
     number

%---Prandtl Number---
Pr_h=cp_he*mu_he(Th_avg_C)/k_he(Th_avg_C);   %Hot fluid Prandtl number (
    average temperature)
Pr_in_h=cp_he*mu_he(Th_i_C)/k_he(Th_i_C);    %Hot fluid Prandtl number (
    inlet temperature)

Pr_c=cp_he*mu_he(Tc_avg_C)/k_he(Tc_avg_C);   %Cold fluid Prandtl number (
    average temperature)
Pr_in_c=cp_he*mu_he(Tc_i_C)/k_he(Tc_i_C);    %Cold fluid Prandtl number (
    inlet temperature)

%---Critical Reynolds Number---
Rey_critical_h=2300*(1+8.6*(IT_id_m/d_curv)^0.45);  %Hot fluid critical
    reynolds number
Rey_critical_c=2300*(1+8.6*(Dh/d_curv)^0.45);       %cold fluid critical
```

```
    reynolds number

%---Constants for Nusselt Number: Schmidt correlation---
m_h=0.5+0.2903*(IT_id_m/d_curv)^0.194;
A_h=(2.2E+04-Rey_h)/(2.2E+04-Rey_critical_h);
m_c=0.5+0.2903*(Dh/d_curv)^0.194;
A_c=(2.2E+04-Rey_c)/(2.2E+04-Rey_critical_c);

%---Friction Factor---
f_h=(0.3164/Rey_h^0.25+0.03*(IT_id_m/d_curv)^0.5)*(mu_he(Th_i_C)/mu_he(
    Th_avg_C))^0.27; %Hot fluid Fanning friction factor
f_c=(0.3164/Rey_c^0.25+0.03*(Dh/d_curv)^0.5)*(mu_he(Tc_i_C)/mu_he(Tc_avg_C)
    )^0.27;  %Cold fluid Fanning friction factor

%===Nusselt Number Correlations===
%---Nusselt number for hot fluid---
if  Rey_h<2300
    Nu_h=3.65+0.08*(1+0.8*(IT_id_m/d_curv)^0.9)*(Rey_h^m_h)*(Pr_h)
        ^(1.0/3.0)*(Pr_h/Pr_in_h)^0.14;
elseif 2300<=Rey_h && Rey_h<22000
    Nu_h=A_h*(3.65+0.08*(1+0.8*(IT_id_m/d_curv)^0.9)*(Rey_critical_h^m_h)*(
        Pr_h)^(1.0/3.0)*(Pr_h/Pr_in_h)^0.14)+(1-A_h)*((f_h/8.0)*22000.0*
        Pr_h)/(1+12.7*sqrt(f_h/8.0)*(Pr_h^(2.0/3.0)-1))*(Pr_h/Pr_in_h)
        ^0.14;
else
    Nu_h=((f_h/8.0)*Rey_h*Pr_h)/(1+12.7*sqrt(f_h/8.0)*(Pr_h^(2.0/3.0)-1))*(
        Pr_h/Pr_in_h)^0.14;
end

%---Nusselt number for cold fluid---
if  Rey_c<2300
    Nu_c=3.65+0.08*(1+0.8*(Dh/d_curv)^0.9)*(Rey_c^m_c)*(Pr_c)^(1.0/3.0)*(
        Pr_c/Pr_in_c)^0.14;
elseif 2300<=Rey_c && Rey_c<22000
    Nu_c=A_c*(3.65+0.08*(1+0.8*(Dh/d_curv)^0.9)*(Rey_critical_c^m_c)*(Pr_c)
        ^(1.0/3.0)*(Pr_c/Pr_in_c)^0.14)+(1-A_c)*((f_c/8.0)*22000.0*Pr_c)
        /(1+12.7*sqrt(f_c/8.0)*(Pr_c^(2.0/3.0)-1))*(Pr_c/Pr_in_c)^0.14;
else
    Nu_c=((f_c/8.0)*Rey_c*Pr_c)/(1+12.7*sqrt(f_c/8.0)*(Pr_c^(2.0/3.0)-1))*(
        Pr_c/Pr_in_c)^0.14;
end

%---Convective heat transfer coefficient---
h_h=Nu_h*k_he(Th_avg_C)/IT_id_m;   %Hot fluid convective heat transfer
    coefficient in W/m^2-C
h_c=Nu_c*k_he(Tc_avg_C)/Dh;        %Cold fluid convective heat transfer
    coefficient in W/m^2-C

%---Overall heat transfer coefficient---
U=(1/h_h+(IT_id_m/2)/k_p*log(IT_od_m/IT_id_m)+(IT_id_m/IT_od_m)*1/h_c)
    ^(-1.0);   %Overall heat transfer coefficient in W/m^2-C
```

```
%---Heat Transfer Area---
A_ht=UA/U;      %Heat transfer area in m2

%---Length of HX---
L=A_ht/(pi*IT_od_m*N);   %Length of HX tubes in m

%---Pressure Drop---
del_P_h=(f_h*(L/IT_id_m)*(rho_he(Th_avg_C)*vel_h^2.0/2))/10^3; %Pressure
   drop in hot fluid in kPa
del_P_c=(f_c*(L/Dh)*(rho_he(Tc_avg_C)*vel_c^2.0/2))/10^3;      %Pressure
   drop in cold fluid in kPa
del_P_max=max(del_P_c,del_P_h); %Maximum calculated pressure drop in kPa

i=i+1;  %Counter increment
N=N+1;  %Number of tubes increment
end

%---Volume Calculations---
CSA=N*pi()*OT_od_m^2/4;     %Cross sectional area of tube bundle in m^2
Volume=CSA*L;               %Volume of HX in m^3
Compactness=A_ht/Volume;    %HX Compactness in m^2/m^3

%---Figures of Merit---
FOM1=U/del_P_max;       %Overall heat transfer coefficient per pressure
   drop
FOM2=del_P_max/L;       %Overall pressure drop per length of HX

%---Pumping Work---
W_cold=del_P_c.*m_cold./rho_he(Tc_avg_C); %Cold side pumping power in kW
W_hot=del_P_h.*m_hot./rho_he(Th_avg_C);   %Hot side pumping power in kW
W_max=max(W_cold,W_hot);

%==================COST ANALYSIS==============================
rho_mat=8360;   %Density of Alloy 617 in kg/m^3
Cost_mat=120;   %Cost of Alloy 617 in $/kg
Cost_elec=0.12; %Cost of electricity in $/kWh
Num_years=10;   %Number of operational years

%---Total HX Material Calculations---
V_ch=pi()*((OT_od_m^2-OT_id_m^2)+(IT_od_m^2-IT_id_m^2))*L/4;   %Volume of a
    single tube's material in m^3
V_mat=V_ch*N;           %Material volume of HX in m^3
M_mat=V_mat*rho_mat;    %Mass of HX material in kg

%---Pricing---
CapCost_HX=M_mat*Cost_mat;                  %Capital cost of HX in USD
OpCost_HX=W_max*Cost_elec*Num_years*24*365; %Operating cost of HX in USD
TotalCost_HX=CapCost_HX+OpCost_HX;          %Total cost of HX in USD

%=====END OF CODE FOR HCHE=====%
%************************************************************************
%************************************************************************
```